

# $\Lambda(1405)$ photoproduction based on chiral unitary model

S.X. Nakamura<sup>1,\*</sup> and D. Jido<sup>2</sup>

<sup>1</sup>*Yukawa Institute for Theoretical Physics,  
Kyoto University, Kyoto, 606-8502, Japan*

<sup>2</sup>*Department of Physics, Tokyo Metropolitan University, Hachioji, Tokyo 192-0397, Japan*

## Abstract

Recent CLAS data for the  $\pi\Sigma$  invariant mass distributions (line-shapes) in the  $\gamma p \rightarrow K^+\pi\Sigma$  reaction are theoretically investigated. The line-shapes have peaks associated with the  $\Lambda(1405)$  excitation. Our model consists of gauge invariant photo-production mechanisms, and the chiral unitary model that gives the rescattering amplitudes where  $\Lambda(1405)$  is contained. It is found that, while the  $\pi\Sigma$  line-shape data in the  $\Lambda(1405)$  region are successfully reproduced by our model for all the charge states, the production mechanism is not so simple that we need to introduce parameters associated with short-range dynamics to fit the data. Our detailed analysis suggests that the nonresonant background contribution is not negligible, and its sizable effect shifts the  $\Lambda(1405)$  peak position by several MeV. We also analyze the data using a Breit-Wigner amplitudes instead of those from the chiral unitary model. We find that the fitted Breit-Wigner parameters are closer to the higher pole position for  $\Lambda(1405)$  of the chiral unitary model. This work sets a starting point for a fuller analysis in which line-shape as well as  $K^+$  angular distribution data are simultaneously analyzed for extracting  $\Lambda(1405)$  pole(s).

PACS numbers: 13.30.Eg, 13.60.Le, 13.60.Rj, 14.20.Gk 14.20.Jn,

arXiv:1310.5768v2 [nucl-th] 3 Feb 2014

---

\* Present address: Department of Physics, Osaka University, Toyonaka, Osaka 560-0043, Japan;  
[nakamura@kern.phys.sci.osaka-u.ac.jp](mailto:nakamura@kern.phys.sci.osaka-u.ac.jp)

## I. INTRODUCTION

The pole structure of the  $\Lambda(1405)$  resonance is a key issue to understand the nature of  $\Lambda(1405)$  and the  $\bar{K}N$  interaction. Because  $\Lambda(1405)$  decays exclusively into the  $\pi\Sigma$  channel with  $I = 0$  by the strong interaction, a signal associated with  $\Lambda(1405)$  is expected to be observed in the  $\pi\Sigma$  invariant mass distributions (to be referred to as “line-shape”) of certain  $\Lambda(1405)$  production reactions.

In old bubble chamber experiments, bumps associated with the  $\Lambda(1405)$  excitation have been observed in the  $\pi\Sigma$  line-shapes of hadron induced reactions, such as  $\pi^-p \rightarrow K^+\pi\Sigma$  [1],  $K^-p \rightarrow \pi^-\pi^+\pi\Sigma$  [2] and  $K^-d \rightarrow n\pi^+\Sigma^-$  [3]. The observed bumps in the first two experiments are consistent with the  $\Lambda(1405)$  resonance at 1405 MeV, while the reaction with a deuteron target found the  $\Lambda(1405)$  resonance at 1420 MeV. Recently, the  $\pi^0\Sigma^0$  line-shape for the  $\Lambda(1405)$  energies was also measured in hadronic reactions, such as  $K^-p \rightarrow \pi^0\pi^0\Sigma^0$  with 514-750 MeV/c kaon momenta by Crystal Ball Collaboration [4], and  $pp \rightarrow pK^+\Lambda(1405)$  with 3.65 GeV/c proton beam at COSY-Jülich [5].

Although there have been several data for the  $\Lambda(1405)$  spectrum from the hadron beam experiments as mentioned above, the quality of the data is still not sufficient for extracting  $\Lambda(1405)$  pole(s). The situation has been changed by recent photon-beam experiments. The first photoproduction of the  $\Lambda(1405)$  resonance was observed at SPring 8 by LEPS collaboration in the  $\gamma p \rightarrow K^+\pi\Sigma$  reaction with the photon energy of 1.5-2.4 GeV [6, 7]. In this experiment, the  $\pi^-\Sigma^+$  and  $\pi^+\Sigma^-$  line-shapes were measured, and they were found to be different from each other, owing to the interference between the  $I = 0$  resonant and  $I = 1$  non-resonant contributions. A high statistics, wide angle coverage experiment for the  $\gamma p \rightarrow K^+\pi\Sigma$  reaction was performed at Jefferson Laboratory by the CLAS collaboration, for center-of-mass energies  $1.95 < W < 2.85$  GeV [8, 9]. In this experiment, all the three charge states of the  $\pi\Sigma$  channels were simultaneously observed in the  $\gamma p$  scattering for the first time, and the differential cross sections were measured for the  $\pi\Sigma$  line-shape and for the  $K^+$  angular distribution. This is the cleanest data that cover the kinematics of  $\Lambda(1405)$  excitation, which encourages theorists to seriously work on extracting the  $\Lambda(1405)$  pole(s) from data for the first time. Very recently the spectral shape of  $\Lambda(1405)$  has been also observed in electroproduction in the range of  $1.0 < Q^2 < 3.0$  (GeV/c)<sup>2</sup> [10].

The coupled-channel approach based on the chiral effective theory (chiral unitary model) suggests that the  $\Lambda(1405)$  resonance is composed of two poles located between the  $\bar{K}N$  and  $\pi\Sigma$  thresholds [11] and these states have different masses, widths and couplings to the  $\bar{K}N$  and  $\pi\Sigma$  channels. One pole is located at  $1426 - 16i$  MeV with a dominant coupling to  $\bar{K}N$ , while the other is sitting at  $1390 - 66i$  MeV with a strong coupling to  $\pi\Sigma$  [12]. These two states are generated dynamically by the attractive interaction in the  $\bar{K}N$  and  $\pi\Sigma$  channels with  $I = 0$  [13]. Because the  $\Lambda(1405)$  resonance is composed of two states which have different weight to couple with  $\bar{K}N$  and  $\pi\Sigma$ , the spectral shape of the  $\pi\Sigma$  line-shape in the  $\Lambda(1405)$  region depends on how  $\Lambda(1405)$  is produced, as pointed out in Ref. [12]. Reference [12] predicts that the  $\Lambda(1405)$  resonance in the  $\bar{K}N \rightarrow \pi\Sigma$  channel has a peak at 1420 MeV with a narrower width because the higher pole strongly couples to the  $\bar{K}N$  channel. The study of Ref. [14] showed that, in the  $K^-d \rightarrow n\pi\Sigma$  reaction,  $\Lambda(1405)$  is dominantly produced by  $\bar{K}N$ , and the  $\pi\Sigma$  line-shape has a peak at 1420 MeV as seen in the old bubble chamber experiment [3].

It is important to confirm the two-pole structure by analyzing the new CLAS data, and if so, it will be interesting to see how the two-pole structure plays a role in the  $\pi\Sigma$  line-shape.

In order to extract the  $\Lambda(1405)$  resonance pole(s) from the production data, we develop a model that consists of production mechanism followed by the final state interaction (FSI);  $\Lambda(1405)$  is excited in the FSI. Through a careful analysis of the data, we can pin down the production mechanism as well as the scattering amplitude responsible for the FSI. Then the  $\Lambda(1405)$  pole(s) will be extracted from the scattering amplitude. Such an analysis of the new CLAS data has been done in Refs. [15, 16] using a simple production mechanism.

In this work, we focus on the photoproduction of  $\Lambda(1405)$  in  $\gamma p \rightarrow K^+ \pi \Sigma$ , and investigate the new CLAS data for the  $\pi \Sigma$  line-shape [8]. The first study of the reaction was done in Ref. [17], in which a simple diagram was considered for the  $\Lambda(1405)$  production mechanism and the  $\Lambda(1405)$  is described by the chiral unitary approach. Related calculations were also done in Refs. [18, 19]. Although the calculation of Ref. [17] was to get a rough estimate of the cross sections, in the advent of the fairly precise data, it is necessary to develop a quantitative model to extract the  $\Lambda(1405)$  properties from the data. In this work, we extend and refine the model of Ref. [17] by considering more production mechanisms that are gauge invariant at the tree-level. We consider relevant meson-exchange mechanisms, and contact terms that simulate short-range mechanisms. We explain details of the model, and successfully fit the CLAS data with it. Then we discuss a role played by each mechanism, effects of non-resonant contributions, and a possibility of a single-pole solution of  $\Lambda(1405)$ . By doing so, we set a starting point for a full analysis in which we simultaneously analyze the data for line-shape [8] and the  $K^+$  angular distribution [9] to study the pole structure of  $\Lambda(1405)$ . Such a full analysis is left to a future work. We expect the  $K^+$  angular distribution data are an important information to pin down the production mechanism.

The rest of this paper is organized as follows: We give a detailed description of our model in Sec. II. Then we show numerical results and discuss them in Sec. III, followed by a summary in Sec. IV. Expressions for Lagrangians and photo-production operators, and also model parameters are collected in Appendices.

## II. MODEL

### A. Kinematics and cross section formula

First we define kinematical variables. We consider the  $\gamma(q)+p(p) \rightarrow K^+(k)+\pi(k_\pi)+\Sigma(p')$  reaction in which the variables in the parentheses are four-momenta for the particles in the total center-of-mass system. The differential cross section for the reaction is derived following a standard procedure, and given as

$$d\sigma = \frac{M_p M_\Sigma \lambda^{1/2}(s, M_{\pi\Sigma}^2, m_{K^+}^2) \lambda^{1/2}(M_{\pi\Sigma}^2, M_\Sigma^2, m_\pi^2)}{512\pi^5 s (s - M_p^2) M_{\pi\Sigma}} \sum_{\text{spin}} |T_{K^+\pi\Sigma, \gamma p}|^2 dM_{\pi\Sigma} d\Omega_k d\Omega_{p'}^* , \quad (1)$$

where  $M_p$ ,  $M_\Sigma$ ,  $m_{K^+}$  and  $m_\pi$  are the masses of the proton,  $\Sigma$ ,  $K^+$  and  $\pi$ , respectively, and the Källén function is denoted by  $\lambda(x, y, z)$ . The symbol  $s$  is the squared total energy of the system, and is related to the four-momenta by  $s = W^2 = (q + p)^2 = (k + k_\pi + p')^2$ , while the invariant mass of the  $\pi\Sigma$  subsystem is  $M_{\pi\Sigma}^2 = (k_\pi + p')^2$ . The kinematical variables with asterisk stand for the quantities in the  $\pi\Sigma$  center-of-mass system. The summation of spin and polarization states in initial and final particles are indicated by  $\sum_{\text{spin}}$ ; the average factor,  $1/4$ , for the initial states is already included in the factor of the formula. All information about the dynamics is encoded into the reaction amplitude  $T_{K^+\pi\Sigma, \gamma p}$  in Eq. (1), and is

discussed in detail in the next subsection. The line-shape of the  $\pi\Sigma$  spectrum is obtained by integrating Eq. (1) over the angular part of  $\vec{p}^*$  and  $\vec{k}$ , and given as

$$\frac{d\sigma}{dM_{\pi\Sigma}} = \sum_{\text{spin}} \int d\Omega_k d\Omega_{p'}^* \frac{M_p M_\Sigma \lambda^{1/2}(s, M_{\pi\Sigma}^2, m_{K^+}^2) \lambda^{1/2}(M_{\pi\Sigma}^2, M_\Sigma^2, m_\pi^2)}{512\pi^5 s (s - M_p^2) M_{\pi\Sigma}} |T_{K^+\pi\Sigma, \gamma p}|^2. \quad (2)$$

## B. Photo-production mechanism

As stated in the introduction, we describe the  $\gamma p \rightarrow K^+\pi\Sigma$  reaction by a set of tree-level mechanisms for  $\gamma p \rightarrow K^+ M_j B_j$  ( $M_j B_j$ : a set of meson and baryon) followed by  $M_j B_j \rightarrow \pi\Sigma$  rescattering. We use an index  $j = 1, \dots, 10$  to specify  $M_j B_j = K^- p, \bar{K}^0 n, \pi^0 \Lambda, \pi^0 \Sigma^0, \eta \Lambda, \eta \Sigma^0, \pi^+ \Sigma^-, \pi^- \Sigma^+, K^+ \Xi^-, K^0 \Xi^0$ , respectively. Thus the reaction amplitude introduced in Eq. (1),  $T^j \equiv T_{K^+ M_j B_j, \gamma p}$ , is given by

$$T^j = \sum_{\alpha} V_{\alpha}^j + T_R^j, \quad (3)$$

where  $V_{\alpha}^j$  is a tree-level photo-production mechanism. In the next paragraph, we specify the tree mechanisms that go into our calculation. The summation of  $\alpha$  runs over all of the tree-level photoproduction mechanisms included in our calculation. Contribution from the rescattering is denoted by  $T_R^j$ . The rescattering amplitude is calculated with a partial wave expansion with respect to the relative motion of  $M_j B_j$ , and  $(J, L) = (1/2, 0)$  and  $(1/2, 1)$  partial waves are considered;  $J$  and  $L$  are the total and orbital angular momenta for  $M_j B_j$ . The partial wave amplitude is given, with the on-shell factorization, by

$$T_{R; JL}^j = \sum_{\alpha} \sum_{j'} T_{JL}^{jj'}(M_{\pi\Sigma}^2) G_{\alpha}^{j'}(M_{\pi\Sigma}^2) V_{\alpha; JL}^{j'}, \quad (4)$$

where  $T_{R; JL}^j$  and  $V_{\alpha; JL}^j$  are partial wave amplitudes of  $T_R^j$  and  $V_{\alpha}^j$ , respectively, and are calculated with the on-shell momenta of relevant particles. More details about the partial wave expansion, including the relation between  $T_{R; JL}^j$  and  $T_R^j$ , are given in Appendix A. For the  $M_{j'} B_{j'} \rightarrow M_j B_j$  scattering amplitudes  $T_{JL}^{jj'}$ , we use those from the chiral unitary model given in Ref. [20] for  $(J, L) = (1/2, 0)$  wave, and in Ref. [21] for  $(J, L) = (1/2, 1)$  wave. The  $(J, L) = (1/2, 0)$  wave contains  $\Lambda(1405)$  as double poles, while the  $(J, L) = (1/2, 1)$  wave does not include any resonance and provide a smooth background. It is turned out that the contribution from the  $(J, L) = (1/2, 1)$  wave rescattering is small. We use the meson-baryon Green function,  $G_{\alpha}^j$ , calculated with the dimensional regularization as follows:

$$G_{\alpha}^j(s) = \frac{2M_{B_j}}{16\pi^2} \left\{ a_{\alpha}^j(\mu) + \ln \frac{M_{B_j}^2}{\mu^2} + \frac{M_{M_j}^2 - M_{B_j}^2 + s}{2s} \ln \frac{M_{M_j}^2}{M_{B_j}^2} \right. \\ \left. + \frac{\bar{q}_j}{\sqrt{s}} \left[ \ln(s - (M_{B_j}^2 - M_{M_j}^2) + 2\bar{q}_j \sqrt{s}) + \ln(s + (M_{B_j}^2 - M_{M_j}^2) + 2\bar{q}_j \sqrt{s}) \right. \right. \\ \left. \left. - \ln(-s + (M_{B_j}^2 - M_{M_j}^2) + 2\bar{q}_j \sqrt{s}) - \ln(-s - (M_{B_j}^2 - M_{M_j}^2) + 2\bar{q}_j \sqrt{s}) \right] \right\}, \quad (5)$$

where  $M_{B_j}$  and  $M_{M_j}$  are the masses of a baryon  $B_j$  and a meson  $M_j$ , respectively, and we use the values listed in the Particle Data Group [22] for the masses. The relative on-shell momentum of  $M_j B_j$  corresponding to  $s$  is denoted by  $\bar{q}_j$ . The symbol  $a_{\alpha}^j(\mu)$  is the

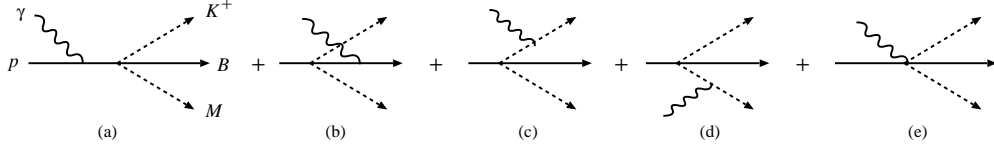


FIG. 1. The gauged Weinberg-Tomozawa terms.

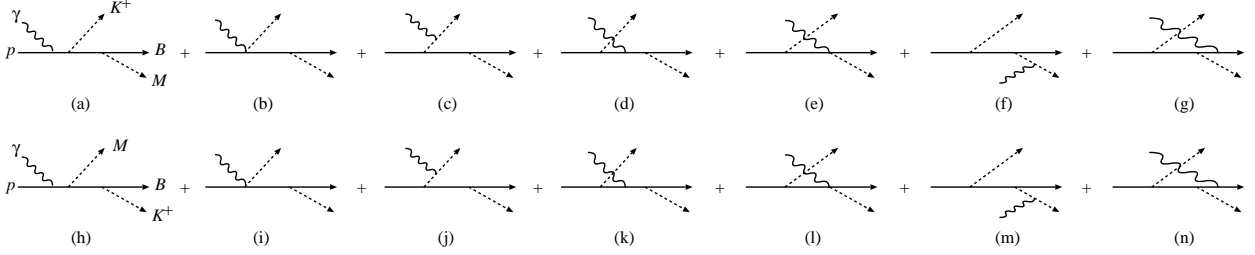


FIG. 2. The gauged Born terms. From the upper row to lower row,  $K^+$  and  $M$  are exchanged.

subtraction constant for the regularization scale  $\mu$ , and we set  $\mu = 630$  MeV for all channels. The subtraction constants can depend on a channel  $j$  as well as a production mechanism  $\alpha$ ; we will come back to this point at the end of this section.

We consider gauge-invariant tree-level photo-production mechanisms ( $V_\alpha^j$ ) as follows: minimal substitution to the lowest order chiral meson-baryon interaction such as the Weinberg-Tomozawa terms (Fig. 1) and the Born terms (Fig. 2); vector-meson exchange mechanisms (Fig. 3). Thus, for specifying each mechanism  $\alpha$ , we use the label for each figure in Figs. 1-3 so that  $\alpha = 1(a), 1(b), \dots, 3(k)$ . These photo-production mechanisms are expanded in terms of  $1/M_B$ , and  $\mathcal{O}(1)$  and  $\mathcal{O}(1/M_B)$  terms are considered in our calculation. Explicit expressions for  $V_\alpha^j$ , as well as our model Lagrangians from which  $V_\alpha^j$  are derived, are shown in Appendix B and C. Coupling constants contained in  $V_\alpha^j$  of Figs. 1-3 are fixed either by data (other than  $\gamma p \rightarrow K^+ \pi \Sigma$ ) if possible, or by SU(3) relation if poorly constrained by data. More details about the couplings are given in Appendix B.

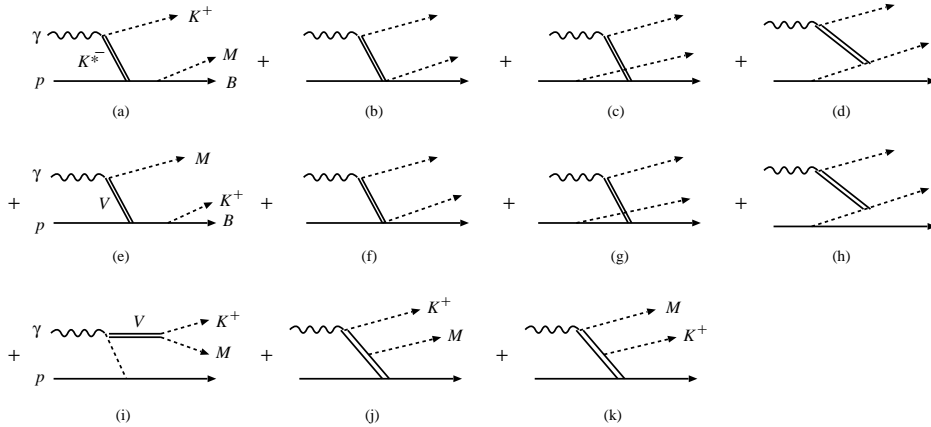


FIG. 3. The vector-meson ( $V$ ) exchange terms. From the first row to second row,  $K^+$  and  $M$  are exchanged.

TABLE I. Classification of production mechanisms. The meson-exchange mechanisms shown in Figs. 1-3 and three contact terms  $c1$ - $c3$  are classified into 11 groups labeled by A,B,...,K. Each group has its own subtraction constants  $a_{\alpha'}^j(\mu)$  in Eq. (5).

	A	B	C	D	E	
$\alpha$	2(a)-(d),3(a), $c1$ , $c2$ , $c3$	1(a),(c),(e)	1(d)	1(b)	2(h)-(j)	
	F	G	H	I	J	K
$\alpha$	2(k)-(n)	2(e),(g)	2(f)	3(b)-(d)	3(e)-(h)	3(i)-(k)

With the meson-exchange production mechanisms and the subtraction constants ( $a_{\alpha'}^j(\mu)$  in Eq. (5)) taken as the same as those in the chiral unitary amplitudes, we cannot reproduce the  $\pi\Sigma$  line-shape data for the  $\gamma p \rightarrow K^+\pi\Sigma$  reaction from the CLAS [8]. Therefore, it is inevitable to introduce adjustable degrees of freedom to fit the data. Thus all of the meson-exchange mechanisms  $V_{\alpha}^j$  are multiplied by a common form factor of the following form:

$$\left( \frac{\Lambda^2}{\Lambda^2 + \mathbf{k}^{*2}} \right) \left( \frac{\Lambda^2}{\Lambda^2 + \mathbf{k}_j^{*2}} \right), \quad (6)$$

where  $\mathbf{k}^*$  and  $\mathbf{k}_j^*$  are respectively the momenta of  $K^+$  and  $M_j$  in the center-of-mass frame of  $M_j B_j$ . The cutoff  $\Lambda$  will be used to fit the data. In addition, we also consider phenomenological contact terms that can simulate mechanisms not explicitly considered, such as, in particular,  $N^*$  and  $Y^*$  excitation mechanisms. We take couplings for the contact terms  $W$ -dependent ( $W$ : total energy of the system), and will be determined by fitting the  $\gamma p \rightarrow K^+\pi\Sigma$  data [8]. We consider three types of contact terms that are gauge-invariant at the tree-level, and are couple to  $K^+\bar{K}N$  and  $K^+\pi\Sigma$  states of different charges, and thus we have 15 complex couplings at each  $W$ . Expressions for the contact terms are presented in Eqs. (C56)-(C58) in Appendix. Also, for the mechanism index  $\alpha$ , we write  $\alpha = c1, c2, c3$ , as in Eqs. (C56)-(C58). The form factor of Eq. (6) is not applied to the contact terms.

The subtraction constants  $a_{\alpha'}^j(\mu)$  included in Eq. (5) are also adjusted to fit the data, thereby changing the interference pattern between different production mechanisms. As already stated,  $a_{\alpha'}^j(\mu)$  can depend on the production mechanism  $\alpha = 1(a), 1(b), \dots, 3(k), c1, c2, c3$ . However, some of  $\alpha$ 's should have the same value for  $a_{\alpha'}^j(\mu)$ . Also, we do not want to have too many free parameters from the subtraction constants, because it will complicate fitting the data. Thus we classify the production mechanisms into several groups, and each group has its own real subtraction constant. In grouping, we try to classify important mechanisms into different groups so that we have effective freedom in fitting. In TABLE I, we show the classification of the mechanisms into 11 groups labeled by A,B,...,K. The subtraction constant for each group is denoted by  $a_{\alpha'}^j(\mu)$  where  $\alpha'$  refers to one of the groups, A,B,...,K. Then  $a_{\alpha'}^j(\mu)$  will be used to fit the data [8]. It is noted that we do not adjust the subtraction constants in the chiral unitary amplitudes in the fit. The subtraction constants we adjusted are all for the first loop of the rescattering, and for the renormalization of the production mechanism.

For the number of data points to be fitted, we now have rather many free parameters most of which are from contact terms. We find that this amount of degrees of freedom is necessary to obtain a reasonable fit to the data. This situation can be understood, considering that



we do not explicitly consider short-range mechanisms (baryon resonances, coupled-channel effects) that will play a substantial role here. Because it will be a very difficult task to identify and/or fix each of the short-range mechanisms, we develop the production model in a practical manner as discussed above. Of course, our method could bring a model-dependence of  $\Lambda(1405)$  pole(s) extracted from the data. The model-dependence of  $\Lambda(1405)$  pole(s) must be assessed by analyzing the data with different form factors and/or contact terms. This will be a future work.

### III. RESULT

#### A. Fitting data

Before presenting our results, we comment on the calculated quantity to be fitted to the line-shape data from CLAS [8]. In the data analysis done by CLAS in Ref. [8], enhanced events due to the  $K^*$  peak in the  $\pi K^+$  invariant mass spectrum has been subtracted. In our model, a mechanism of Fig. 3(i) without rescattering can create the  $K^*$  peak. Thus we fit the data with the following modified differential cross section:

$$\frac{d\sigma}{dM_{\pi\Sigma}}(\text{full}) - \frac{d\sigma}{dM_{\pi\Sigma}}(V_{3(i)}^{\pi\Sigma}), \quad (7)$$

where  $\frac{d\sigma}{dM_{\pi\Sigma}}(\text{full})$  contains all of the meson-exchange mechanisms and contact terms followed by the rescattering as discussed in Sec. II B, and is calculated using Eq. (2). Meanwhile, the second term  $\frac{d\sigma}{dM_{\pi\Sigma}}(V_{3(i)}^{\pi\Sigma})$  contains only the tree-level mechanism of Fig. 3(i). The subtraction in Eq. (7) is done at the cross section level, and the interference between the mechanism of Fig. 3(i) and others is kept to be consistent with the analysis of Ref. [8].

We present all numerical values for the fitting parameters (the cutoff from the form factor, the subtraction constants, and the complex couplings from the contact terms) in Appendix D.

#### B. Line-shape results

Our results, after the fit, are presented in Fig. 4 where the CLAS data are also shown for comparison. We fitted the data at  $W = 2.0, 2.1, 2.2$  and  $2.3$  GeV. As seen in the figure, our model fits the data very well for all three different charge states of  $\pi\Sigma$ .

It is interesting to break down the line-shapes into contributions from different mechanisms, as shown in Fig. 5. As seen in the figures, different mechanisms gives significant contributions that interfere with each other. We find that the contributions from the gauged Weinberg-Tomozawa terms (Fig. 1) are rather small. In fact, a diagram such as Fig. 1(e) gives a contribution comparable to those from the gauged Born mechanisms (Fig. 2). However, as a result of a destructive interference, the net contribution from the gauged Weinberg-Tomozawa terms is rather small. This destructive interference is not necessarily a result of the gauge invariance. Actually, a dominant term in Fig. 1(e) is gauge invariant itself. Rather, fitting the data have fixed relevant subtraction constants so that the diagrams in Fig. 1 with the rescattering cancel out each other. We find relatively large contributions from mechanisms of Fig. 1(e), 2(b), 2(e), 2(i), 2(l), 3(b), 3(f), that have two propagators rather than three in the other mechanisms; the propagators tend to suppress the contributions of

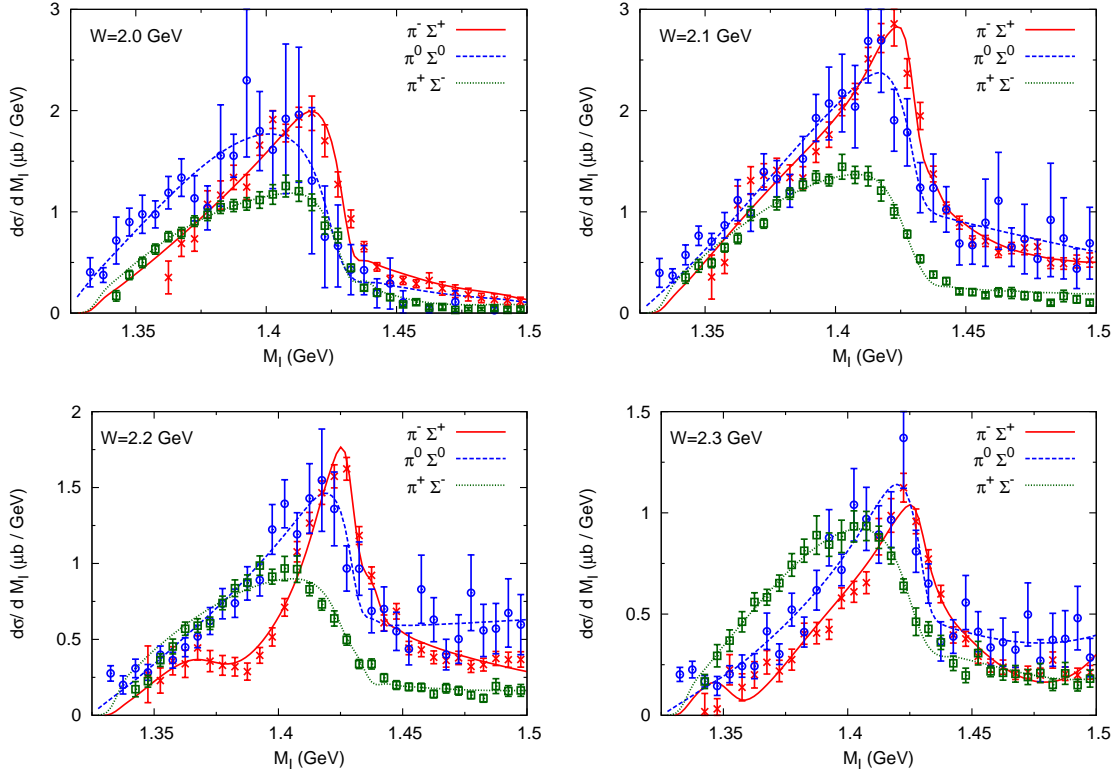


FIG. 4. (Color online) Comparison of  $\pi\Sigma$  line-shapes from our model with data [8] at  $W = 2.0, 2.1, 2.2$  and  $2.3$  GeV. Symbols for the data are cross (red) for  $\pi^-\Sigma^+$ , circle (blue) for  $\pi^0\Sigma^0$ , and square (green) for  $\pi^+\Sigma^-$ .

the mechanisms. Meanwhile, the contact terms, which simulate short-range dynamics, also give a large contribution to bring the theoretical calculation into agreement with the data. As seen in TABLE IV, the contact terms have a rather strong coupling to the  $\bar{K}N$  channels as a result of the fit. One may find in TABLE IV that the  $W$ -dependence of the contact couplings is rather irregular, and is not well under control. However, we note that the contact terms can have a resonant behavior. Also, in Fig. 6, we show the  $W$ -dependence of the most important contact couplings,  $\lambda_1^j$  and  $\lambda_2^j$  for  $j = K^-p$  and  $\bar{K}^0n$ . From the figure, it is hard to judge if the behavior of the couplings is out of control. As will be discussed later, however, we would be able to put them under better control if we fit not only the line-shape data but also other observables such as angular distributions. This will be a future work. Finally, we mention that coupled-channels effects are mostly from the  $\bar{K}N$  and  $\pi\Sigma$  channels.

The difference in the line-shape between different charge states observed in Fig. 4 is a result of the interference between different isospin states. The  $\pi\Sigma$  has three isospin states ( $I = 0, 1, 2$ ), and they are separately shown in Fig. 7. A dominant contribution is from the  $I = 0$  state as expected due to the  $\Lambda(1405)$  peak. The higher mass pole at  $1426 - 16i$  MeV, that creates the prominent bump in the line-shapes, seems to play more important role than the lower mass pole. This is because the production mechanisms in our model generate  $\bar{K}N$  more strongly than  $\pi\Sigma$ , and the final state interaction induces  $\bar{K}N \rightarrow \pi\Sigma$ . As shown in the previous study [12], the higher mass pole couples to the  $\bar{K}N$  channel more strongly than the



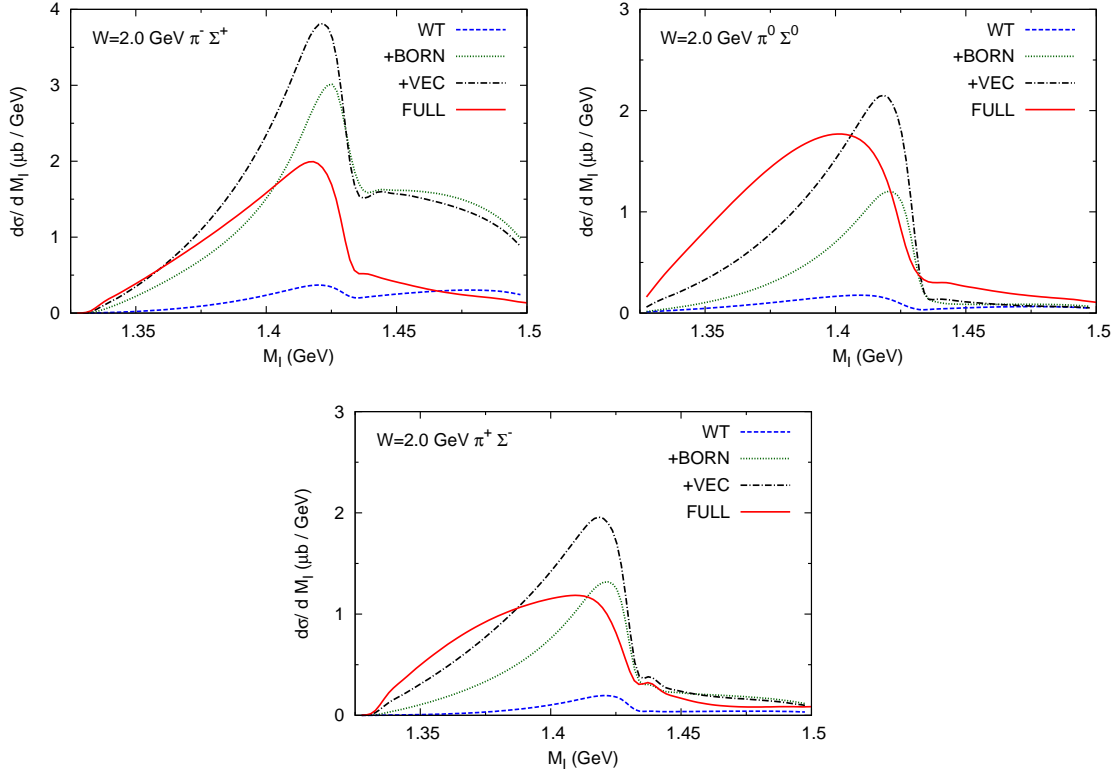


FIG. 5. (Color online) Contribution of each production mechanism. Contribution from the gauged Weinberg-Tomozawa terms (Fig. 1) is given by the blue dashed lines. Contribution that additionally includes the gauged Born terms (Fig. 2) is given by the green dotted lines. Contribution that further includes the vector-meson exchange terms (Fig. 3) is given by the black dash-dotted lines. Finally, the full result, including the contact terms, is shown by the red solid lines.

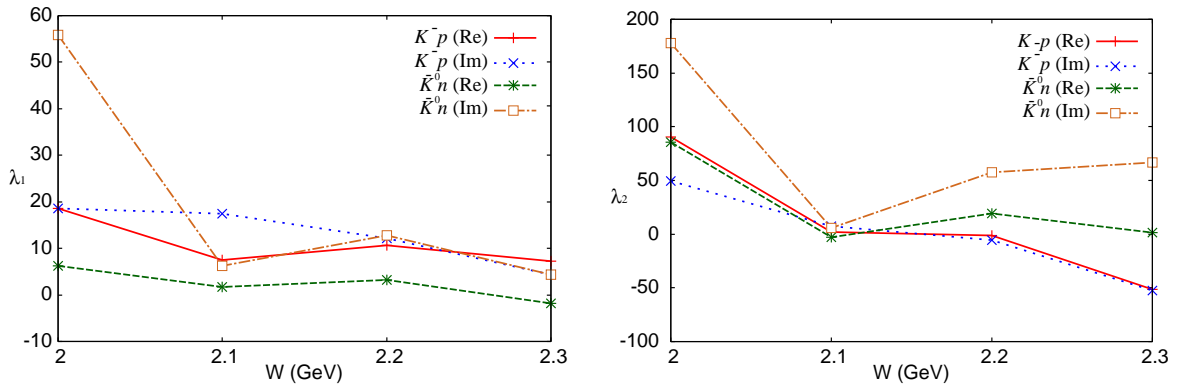


FIG. 6. (Color online) The  $W$ -dependence of the contact couplings,  $\lambda_1^j$  (left) and  $\lambda_2^j$  (right) for  $j = K^-p$  and  $\bar{K}^0n$ . The contact terms are defined in Eqs. (C56)-(C58). The real and imaginary parts of the couplings are indicated by (Re) and (Im), respectively.

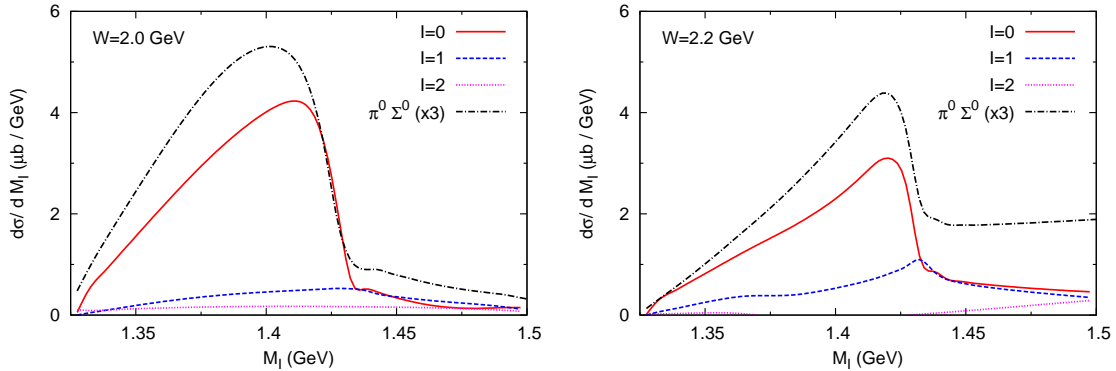


FIG. 7. (Color online) Isospin decomposition of  $\pi\Sigma$  line-shapes. Contributions from the total isospin state  $I$  are shown, along with the line-shape of  $\pi^0\Sigma^0$  multiplied by 3.

lower mass pole does. The  $I = 1$  state gives a smaller contribution, still plays an important role to generate the charge dependence of the  $\pi\Sigma$  line-shapes. As the energy  $W$  increases, the  $I = 1$  contribution is larger. The  $I = 2$  state contribution is even more smaller, but still unnegligible. To see this point, we show in Fig. 7 the  $\pi^0\Sigma^0$  line-shape multiplied by 3. The difference between this and the  $I = 0$  line-shape is the effect of the interference between the  $I = 0$  and  $I = 2$  states. We can see that the interference with the  $I = 2$  state even changes slightly the peak position of the  $\pi^0\Sigma^0$  line-shape.

The different peak positions for differently charged  $\pi\Sigma$  states seen in Fig. 4 can be also understood as a result of the interference between a resonant and a background parts. To see this, it is useful to decompose the amplitude into the resonant (second term of Eq. (3)) and background (first term of Eq. (3)) parts. Each of the contributions to  $\gamma p \rightarrow K^+\pi\Sigma$  at  $W = 2.0$  GeV is shown in Fig. 8. Interestingly, the background terms give smooth and significant contributions. Although the peak structures are due to the resonant contributions, the background can shift the positions of the peaks, particularly the peak of the  $\pi^0\Sigma^0$  line-shape. After all, the resonant contributions give the peaks at almost the same position,  $M_{\pi\Sigma} \sim 1.42$  GeV, for all the differently charged  $\pi\Sigma$  states. Thus it seems that one of the  $\Lambda(1405)$  poles at  $1426 - 16i$  MeV plays a dominant role in the line-shapes. We will look into this observation in the next subsection.

### C. Single Breit-Wigner model

So far, the excitation of  $\Lambda(1405)$  is described by the chiral unitary model, and  $\Lambda(1405)$  has the double-pole structure. However, as seen above, only the higher mass pole seems to give the dominant contribution. Thus, it is interesting to see if a single Breit-Wigner can simulate the photo-induced  $\Lambda(1405)$  excitation. For this purpose, we use a model in which the rescattering amplitude,  $T_{JL}^{jj'}$  in Eq. (4), is given by, instead of the chiral unitary amplitude, a single Breit-Wigner function in  $(J, L) = (1/2, 0)$  and isospin zero partial wave; the other rescattering partial waves amplitudes are set to zero. Here we assume that the rescattering amplitude couples to only  $\bar{K}N$  and  $\pi\Sigma$  channels. Thus we have

$$T_{1/2,0}^{jj'}(s) = \frac{C_{jj'}^{BW}}{\sqrt{s} - M_{BW} + i\frac{\Gamma_{BW}}{2}}, \quad (8)$$

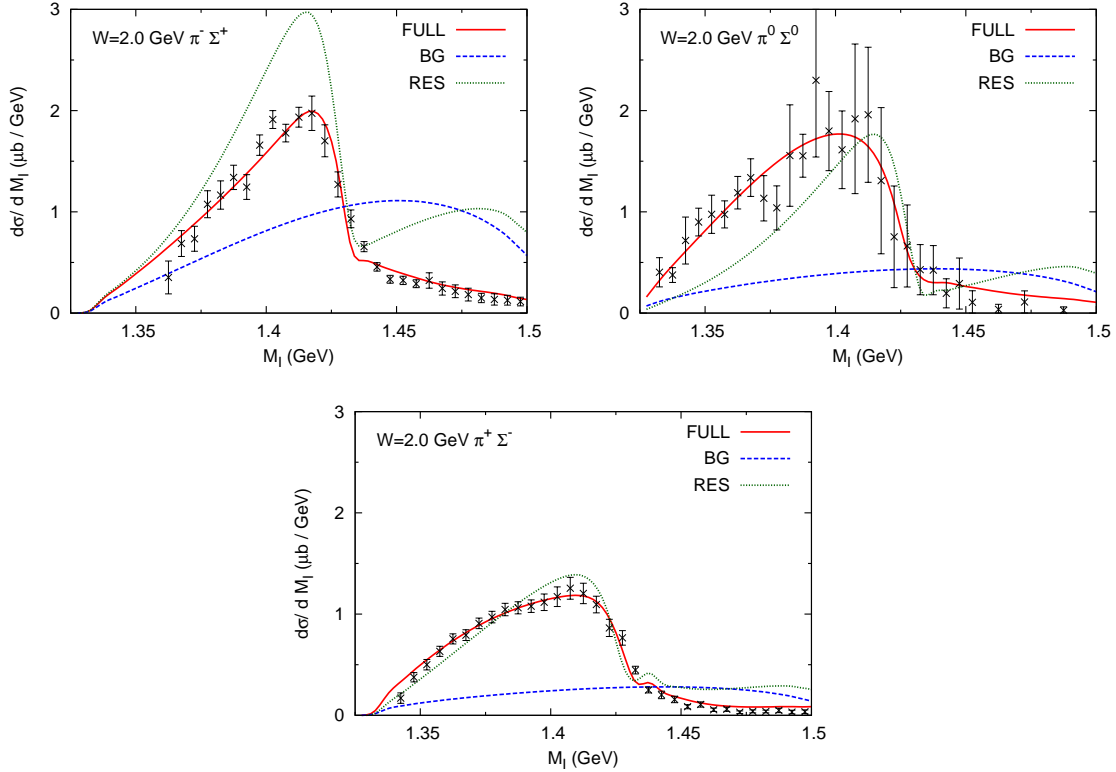


FIG. 8. (Color online) Contribution of background (BG) and resonant (RES) terms. Contribution of the background contribution is from first term of Eq. (3) while the resonant contribution is from second term of Eq. (3). Coherent sum of 'BG' and 'RES' is given by 'FULL', and is compared with data [8].

where  $M_{BW}$  and  $\Gamma_{BW}$  are Breit-Wigner mass and width, respectively. A symbol  $C_{jj'}^{BW}$  is a complex coupling strength, and will be fitted to the data, along with the Breit-Wigner mass, width and other fitting parameters. Because of being isospin zero,  $C_{jj'}^{BW}$  have three independent complex values that we denote  $C_{\bar{K}N, \bar{K}N}^{BW}$ ,  $C_{\bar{K}N, \pi\Sigma}^{BW}$ , and  $C_{\pi\Sigma, \pi\Sigma}^{BW}$ :  $C_{\bar{K}N, \bar{K}N}^{BW}$  is for  $(j, j') = (1 \text{ or } 2, 1 \text{ or } 2)$ ;  $C_{\bar{K}N, \pi\Sigma}^{BW}$  is for  $(j, j')$  or  $(j', j) = (4 \text{ or } 7 \text{ or } 8, 1 \text{ or } 2)$ ;  $C_{\pi\Sigma, \pi\Sigma}^{BW}$  is for  $(j, j') = (4 \text{ or } 7 \text{ or } 8, 4 \text{ or } 7 \text{ or } 8)$ . We have defined the index  $j$  at the beginning of Sec. II B. Our Breit-Wigner form of Eq. (8) is more relaxed than the conventional one in which the coupling strengths are related to the width by  $\Gamma_{BW} = \sum_j \delta(\sqrt{s} - \sqrt{s_j}) C_{jj'}^{BW}$ , where the summation is taken over both channels and their particles' phase-space. In this way, we can simulate non-resonant effects that are not considered explicitly in the rescattering amplitude. The single Breit-Wigner model is fitted to the data and is shown with the data in Fig. 9. The fitted parameters are presented in tables in Appendix D. Although the quality of the fit is a little worse than the previous model with the chiral unitary amplitude (Fig. 4), still it is an acceptable level. Thus, the line-shape data for  $\gamma p \rightarrow K^+ \pi \Sigma$  only do not rule out the possibility of single pole solution for  $\Lambda(1405)$ . The fit gives  $M_{BW} = 1412$  MeV and  $\Gamma_{BW} = 67$  MeV that are close to the middle of the two poles from the chiral unitary amplitude, but still closer to the higher mass pole than to the lower one. As seen in TABLE V, the Breit-Wigner amplitude couples strongly (weakly) to the  $\bar{K}N$  ( $\pi\Sigma$ ) channel, which is also similar to the character of the higher mass pole of  $\Lambda(1405)$  in the chiral unitary model.

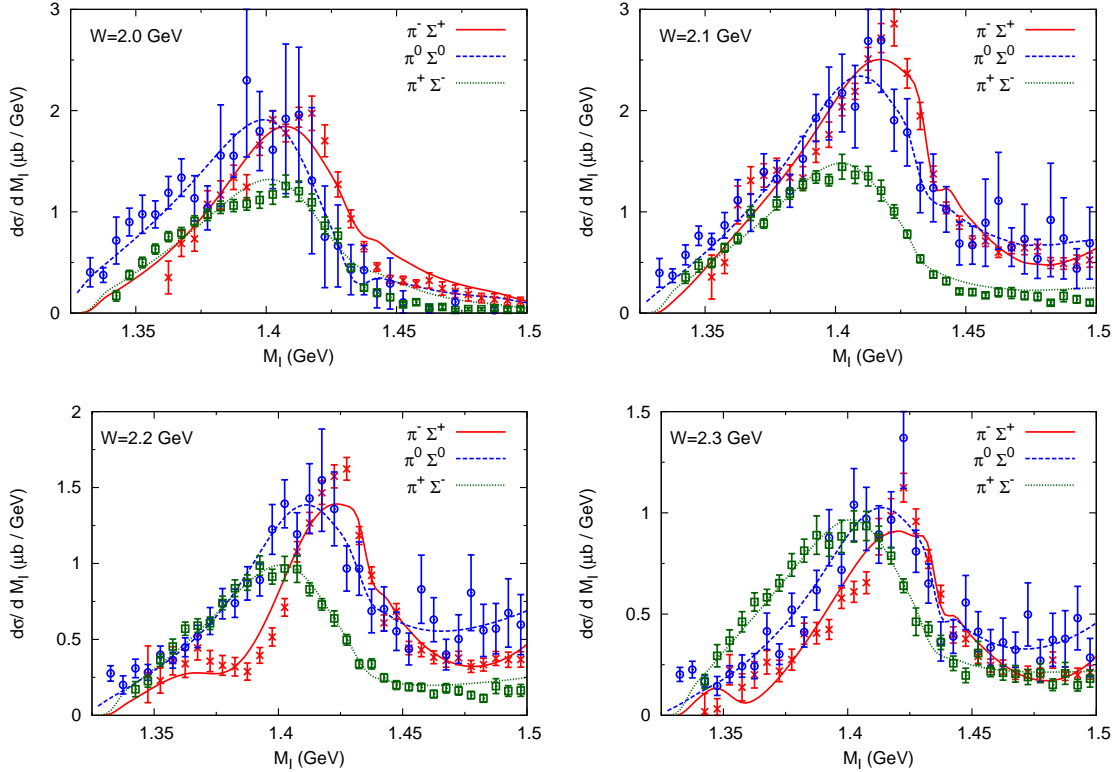


FIG. 9. (Color online) Comparison of  $\pi\Sigma$  line-shapes from single Breit-Wigner model with data [8] at  $W = 2.0, 2.1, 2.2$  and  $2.3$  GeV. See also the caption in Fig. 4.

#### D. $K^+$ angular distribution

So far, we fitted only the  $\pi\Sigma$  line-shape data for the  $\gamma p \rightarrow K^+\pi\Sigma$  reaction. We found that fitting only the  $\pi\Sigma$  line-shape data can lead to several solutions whose quality of the fit to the line-shape data are comparable. However, they can have very different  $K^+$  angular distribution. Therefore,  $K^+$  angular distribution data will be useful information to constrain the production mechanism. Recently the CLAS Collaboration reported data for the  $K^+$  angular distributions [9]. In Figs. 4-8, we actually presented the  $\pi\Sigma$  line-shapes from the model that gives  $K^+$  angular distributions relatively close to the new data of Ref. [9]. Here we use the same model to calculate the  $K^+$  angular distributions, and show them in Fig. 10. At  $W = 2.2$  GeV, our model captures overall trend of the data. However, for the  $\gamma p \rightarrow K^+\pi^0\Sigma^0$  reaction at  $W = 2.0$  GeV, there is a sharp rise in the data at  $\cos\theta \sim 0$  while rather smooth behavior is found in the calculated counterpart. We actually tried fitting the  $K^+$  angular distributions data, but this sharply rising behavior cannot be fitted with the current setup. It seems that we need to search for a mechanism that is responsible for this behavior. We leave such a more detailed analysis of the  $K^+$  angular distribution to a future work.

## IV. SUMMARY

We calculated the  $\pi\Sigma$  line-shapes of the photoproduction process  $\gamma p \rightarrow K^+\pi\Sigma$ . This was motivated by the recent CLAS collaboration's report [8] that found peaks due to  $\Lambda(1405)$

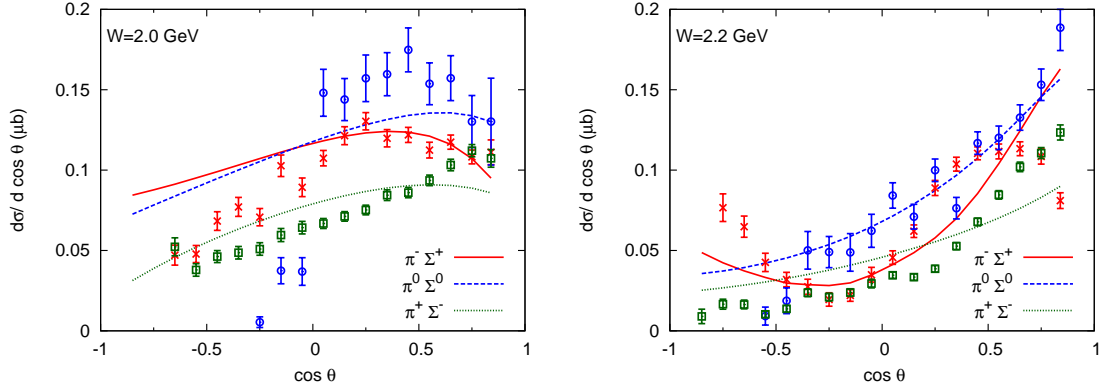


FIG. 10. (Color online) Comparison of the  $K^+$  angular distributions for  $\gamma p \rightarrow K^+ \pi \Sigma$  at  $W = 2.0, 2.2$  GeV with data from the CLAS [9]. See also the caption in Fig. 4.

excitation in the  $\pi \Sigma$  line-shapes. We employed the scattering amplitudes from the chiral unitary model to describe the final state interaction where the  $\Lambda(1405)$  is excited. For the tree-level photo-production mechanisms, we introduced a gauge invariant model that consists of the gauged Weinberg-Tomozawa terms, the gauged Born terms and the vector-meson exchange terms. We also introduced freedom to fit the data such as contact terms modelling short-range dynamics like baryon resonances, and subtraction parameters that can be different from those determined in the chiral unitary model. These are necessary to reproduce the  $\pi \Sigma$  line-shape data from the CLAS. This implies that the mechanism for the  $\Lambda(1405)$  photo-production is not so simple that the several important terms interfere. It is noted that we do not adjust any parameters (subtraction constants, couplings) of the chiral unitary amplitudes in the fit.

Our model reproduces the  $\pi \Sigma$  line-shape data quite well. Breaking down the calculated  $\pi \Sigma$  line-shape into contributions from each production mechanism, we found that the contribution from the gauged Weinberg-Tomozawa terms is not so important due to rather destructive interference between the terms. More important contributions are from the born and vector-meson exchange terms. In addition, the short range contact terms give large contributions to reproduce the  $\pi \Sigma$  line-shape data. We also decomposed the calculated  $\pi \Sigma$  line-shapes into the resonant and nonresonant parts for each charge state of the  $\pi \Sigma$  channels. We found that even though the resonant part dominates the spectra and generates the peak structure, the nonresonant background contribution is not so negligible and its sizable effect shifts the  $\Lambda(1405)$  peak position. The direction of the shift is a consequence of complicated interference of many terms and it is hard to pin down the main mechanism for the shift. One can say that it is not the case that the shift is solely caused by an interference between the  $I = 0$  and  $I = 1$  components, because one can see the shift of the peak position also in the  $\pi^0 \Sigma^0$  channel.

We also made a check of the  $\Lambda(1405)$  amplitude obtained by the chiral unitary model. We refitted the  $\pi \Sigma$  line-shape data with a single Breit-Wigner amplitude for the  $\Lambda(1405)$  amplitude instead of those from the chiral unitary model. The quality of the fit is fairly good, indicating that the  $\pi \Sigma$  line-shape data alone do not rule out a one-pole solution for  $\Lambda(1405)$ . We found that the Breit-Wigner mass and width obtained by the fit are closer to the higher pole position of the  $\Lambda(1405)$  in the chiral unitary model. Also the Breit-Wigner amplitude strongly couples to the  $\bar{K} N$  channel, sharing the similar property of the higher

mass pole. This implies that, in the model including the chiral unitary amplitude, the higher  $\Lambda(1405)$  resonance pole plays a more important role for the photoproduction.

In future work, we will simultaneously analyze data for the  $\pi\Sigma$  line-shape and the  $K^+$  angular distribution, and then extract  $\Lambda(1405)$  pole(s). We presented the  $K^+$  angular distribution from the current model obtained by fitting only the line-shape data. Although our model captures overall behavior of the data in many cases, there is also a qualitative difference that cannot be fixed by fitting with the current setup. Identifying a mechanism that can fill the difference will be a challenge in the future work. Also an important task is to address a model-dependence of the extracted  $\Lambda(1405)$  pole(s) because we are using a rather phenomenological production mechanisms. This can be done by using contact terms and/or form factors of different forms.

## ACKNOWLEDGMENTS

We thank Reinhard Schumacher and Kei Moriya for useful discussions. SXN is the Yukawa Fellow and his work is supported in part by Yukawa Memorial Foundation, by the Yukawa International Program for Quark-hadron Sciences (YIPQS), and by Grants-in-Aid for the global COE program The Next Generation of Physics, Spun from Universality and Emergence from MEXT. This work was partially supported by the Grants-in-Aid for Scientific Research (No. 25400254 and No. 24105706).

## Appendix A: Partial wave expansion

We summarize a partial wave expansion of an amplitude for the  $\gamma + p \rightarrow K^+ + M + B$  ( $M$ : meson;  $B$ : baryon) reaction in the center-of-mass system of  $MB$ , with respect to the relative motion of  $MB$ . We denote the amplitude by  $T$  and its partial wave  $T_{JL}$  where  $J$  and  $L$  are total and orbital angular momenta of  $MB$ , respectively. Here we show equations for the partial waves relevant to this work;  $L = 0, 1$ .

The relation between  $T_{JL}$  and  $T$  for  $(J, L)=(1/2,0)$  is

$$T_{JL} = \frac{1}{4\pi} \int d\Omega_{\hat{\mathbf{k}}_M} T \quad (\text{A1})$$

where  $\mathbf{k}_M$  is the momentum for  $M$  and  $\hat{\mathbf{k}}_M = \mathbf{k}_M/|\mathbf{k}_M|$ . For  $(J, L)=(1/2,1)$ , we have

$$T_{JL} = \frac{1}{4\pi} \int d\Omega_{\hat{\mathbf{k}}_M} \boldsymbol{\sigma} \cdot \hat{\mathbf{k}}_M T , \quad (\text{A2})$$

and for  $(J, L)=(3/2,1)$ ,

$$\mathbf{T}_{JL} \cdot \mathbf{n} = \frac{1}{4\pi} \int d\Omega_{\hat{\mathbf{k}}_M} 3\mathbf{S} \cdot \hat{\mathbf{n}} \mathbf{S}^\dagger \cdot \hat{\mathbf{k}}_M T , \quad (\text{A3})$$

where  $\mathbf{n}$  is an arbitrary vector. The operator  $S^\dagger$  ( $S$ ) is a baryon spin transition operator from spin 1/2 to 3/2 (3/2 to 1/2), and it can be expressed by

$$\mathbf{S} \cdot \mathbf{a} \mathbf{S}^\dagger \cdot \mathbf{b} = \frac{2}{3} \mathbf{a} \cdot \mathbf{b} - \frac{i}{3} \boldsymbol{\sigma} \cdot \mathbf{a} \times \mathbf{b} . \quad (\text{A4})$$



With the partial wave amplitudes  $T_{JL}$  defined above, the original amplitude  $T$  is written as

$$T = T_{1/2,0} + T_{1/2,1} \boldsymbol{\sigma} \cdot \hat{\mathbf{k}}_M + \mathbf{T}_{3/2,1} \cdot \hat{\mathbf{k}}_M + (\text{higher partial waves}) . \quad (\text{A5})$$

A partial wave expansion of production potentials [ $V_\alpha^j$  in Eq. (3)] can be done in the same manner, leading to  $V_{\alpha;JL}^j$  in Eq. (4).

## Appendix B: Model Lagrangians

We present a set of Lagrangians from which we derive photo-production mechanisms graphically shown in Figs. 1-3. We follow the convention of Bjorken-Drell. We use symbols  $B$ ,  $M$ ,  $V$  and  $A$  to denote octet baryon, octet meson, nonet vector meson, and electromagnetic fields, respectively. Also, we use curly symbols to denote creation or annihilation operators. For example,  $\mathcal{B}$  is the annihilation operator contained in  $B$ , and its normalization is  $\langle 0|\mathcal{B}|B\rangle = 1$ .

### 1. Hadronic interactions

We work with the lowest order chiral Lagrangian for the octet pseudoscalar mesons ( $M$ ) coupled to the octet  $1/2^+$  baryons ( $B$ ), as given by <sup>1</sup>

$$\begin{aligned} \mathcal{L}_\chi = & \langle \bar{B} i \gamma^\mu \nabla_\mu B \rangle - M_B \langle \bar{B} B \rangle \\ & + \frac{1}{2} D \langle \bar{B} \gamma_5 \gamma^\mu \{u_\mu, B\} \rangle + \frac{1}{2} F \langle \bar{B} \gamma_5 \gamma^\mu [u_\mu, B] \rangle , \end{aligned} \quad (\text{B1})$$

where the symbol  $\langle \rangle$  denotes the trace of SU(3) flavor matrices,  $M_B$  is the baryon mass and

$$\begin{aligned} \nabla_\mu B &= \partial_\mu B + [\Gamma_\mu, B] , \\ \Gamma_\mu &= \frac{1}{2} (u^\dagger \partial_\mu u + u \partial_\mu u^\dagger) , \\ U &= u^2 = \exp(i\sqrt{2}M/f) , \\ u_\mu &= iu^\dagger \partial_\mu U u^\dagger . \end{aligned} \quad (\text{B2})$$

For the couplings  $D$  and  $F$ , we use  $D = 0.85$ ,  $F = 0.52$ , and  $f = 1.15f_\pi$  with  $f_\pi = 93$  MeV.

The meson and baryon fields in the SU(3) matrix form are

$$M = \begin{pmatrix} \frac{1}{\sqrt{2}}\pi^0 + \frac{1}{\sqrt{6}}\eta & \pi^+ & K^+ \\ \pi^- & -\frac{1}{\sqrt{2}}\pi^0 + \frac{1}{\sqrt{6}}\eta & K^0 \\ K^- & \bar{K}^0 & -\frac{2}{\sqrt{6}}\eta \end{pmatrix} , \quad (\text{B3})$$

$$B = \begin{pmatrix} \frac{1}{\sqrt{2}}\Sigma^0 + \frac{1}{\sqrt{6}}\Lambda & \Sigma^+ & p \\ \Sigma^- & -\frac{1}{\sqrt{2}}\Sigma^0 + \frac{1}{\sqrt{6}}\Lambda & n \\ \Xi^- & \Xi^0 & -\frac{2}{\sqrt{6}}\Lambda \end{pmatrix} . \quad (\text{B4})$$

---

<sup>1</sup> When  $B$ ,  $V$ , and  $M$  are enclosed by the trace brackets, they are SU(3) matrix. Otherwise, they are understood to be one of particles contained in the SU(3) matrix elements. The same applies to the curly symbols for those fields.

From Eq. (B1), we will particularly use the  $BBMM$  interaction, as contained in the covariant derivative, given by

$$\mathcal{L}_{BBMM} = \left\langle \bar{B} i \gamma^\mu \frac{1}{4f^2} [(M \partial_\mu M - \partial_\mu M M) B - B (M \partial_\mu M - \partial_\mu M M)] \right\rangle, \quad (\text{B5})$$

and also use the  $BBM$  interaction, as in  $D$  and  $F$  terms, as

$$\mathcal{L}_{BBM} = -\sqrt{2} g_{PS}^{\text{oct}} \left( \alpha_{PS} \langle \bar{B} \gamma_5 \gamma^\mu B \partial_\mu M \rangle_F + (1 - \alpha_{PS}) \langle \bar{B} \gamma_5 \gamma^\mu B \partial_\mu M \rangle_D \right), \quad (\text{B6})$$

where  $g_{PS}^{\text{oct}} = (D + F)/(2f)$  and  $\alpha_{PS} = F/(D + F)$ , and we have introduced the traces  $\langle \rangle_F$  and  $\langle \rangle_D$  defined by

$$\langle \bar{B} B M \rangle_F = \langle \bar{B} [M, B] \rangle \quad (\text{B7})$$

$$\langle \bar{B} B M \rangle_D = \langle \bar{B} \{M, B\} \rangle - \frac{2}{3} \langle \bar{B} B \rangle \langle M \rangle. \quad (\text{B8})$$

We will also use a notation defined by

$$\langle \bar{B} B M \rangle_S = \langle \bar{B} B \rangle \langle M \rangle. \quad (\text{B9})$$

From here, we discuss interactions involving the nonet vector mesons. In the  $SU(3)$  matrix form, the vector meson nonet is given by

$$V = \begin{pmatrix} \frac{1}{\sqrt{2}} \rho^0 + \frac{1}{\sqrt{2}} \omega & \rho^+ & K^{*+} \\ \rho^- & -\frac{1}{\sqrt{2}} \rho^0 + \frac{1}{\sqrt{2}} \omega & K^{*0} \\ K^{*-} & \bar{K}^{*0} & \phi \end{pmatrix}, \quad (\text{B10})$$

where the ideal mixing between the neutral vector mesons is assumed. With the matrix, the  $VMM$  interactions we use are

$$\mathcal{L}_{VMM} = -i\sqrt{2}g \langle V_\mu (\partial^\mu M M - M \partial^\mu M) \rangle, \quad (\text{B11})$$

where the coupling  $g$  is related to the  $\rho\pi\pi$  coupling by  $g_{\rho\pi\pi} = 2g$ , and we use  $g_{\rho\pi\pi} = 6.0$  determined from the  $\rho \rightarrow \pi\pi$  decay width. The vector part of the  $BBV$  interactions are given by

$$\mathcal{L}_{BBV}^v = -\sqrt{2} g_V^{\text{oct}} \left( \alpha_V \langle \bar{B} \gamma^\mu B V_\mu \rangle_F + (1 - \alpha_V) \langle \bar{B} \gamma^\mu B V_\mu \rangle_D \right) - \frac{g_V^{\text{sin}}}{\sqrt{3}} \langle \bar{B} \gamma^\mu B V_\mu \rangle_S. \quad (\text{B12})$$

We use the coupling constants  $g_V^{\text{oct}} = g = g_{\rho NN}$ , and  $\alpha_V = 1$  from the universality assumption. The relative phase between the  $VMM$  and  $BBV$  interactions is also fixed by the universality. We also use  $g_V^{\text{sin}} = \sqrt{6} g_V^{\text{oct}}$ , so that  $g_{\phi NN} = 0$  and  $g_{\omega NN} = 3g_{\rho NN}$ . The  $BBV$  interactions also contain the tensor coupling, as seen in the common expressions for the  $\rho NN$  and  $\omega NN$  interactions:

$$\mathcal{L}_{\rho NN} = -g_{\rho NN} \left( \bar{N} \gamma^\mu \boldsymbol{\tau} N \cdot \boldsymbol{\rho}_\mu - \frac{\kappa_\rho}{2M_p} \bar{N} \sigma^{\mu\nu} \boldsymbol{\tau} N \cdot \partial_\nu \boldsymbol{\rho}_\mu \right), \quad (\text{B13})$$

$$\mathcal{L}_{\omega NN} = -g_{\omega NN} \left( \bar{N} \gamma^\mu N \omega_\mu - \frac{\kappa_\omega}{2M_p} \bar{N} \sigma^{\mu\nu} N \partial_\nu \omega_\mu \right), \quad (\text{B14})$$

where  $M_p$  is the proton mass. We use  $\kappa_\rho = 2$  and  $\kappa_\omega = 0$ , based on an average of  $\pi N$  and  $\gamma N$  reaction models [23]. The tensor couplings for the other vector mesons are fixed using the SU(3) relation for the magnetic coupling, and an explicit expression will be given later in Eq. (B30). The  $BBVM$  interactions are given by

$$\mathcal{L}_{BBVM} = 2ig_V^{\text{oct}} g_{PS}^{\text{oct}} \left( \alpha_{PS} \left\langle \bar{B} \gamma_5 \gamma^\mu B [M, V_\mu] \right\rangle_F + (1 - \alpha_{PS}) \left\langle \bar{B} \gamma_5 \gamma^\mu B [M, V_\mu] \right\rangle_D \right). \quad (\text{B15})$$

The  $VVM$  interactions we use are based on the hidden local symmetry model [24], and are given by

$$\mathcal{L}_{VVM} = g^2 C \epsilon^{\alpha\beta\gamma\delta} \langle \partial_\alpha V_\beta \partial_\gamma V_\delta M \rangle, \quad (\text{B16})$$

where  $C = -3/(2\sqrt{2}\pi^2 f)$ , and we use the convention,  $\epsilon^{0123} = +1$ .

## 2. Electromagnetic interactions

The photon coupling to the baryonic current is given by

$$L_{\gamma BB'} = -e \bar{B} \left[ Q_{BB'} \not{A} - \frac{\kappa_{BB'}}{2M_p} \sigma^{\mu\nu} (\partial_\nu A_\mu) \right] B'. \quad (\text{B17})$$

The symbol  $Q_{BB'}$  is the electric charge (in unit of  $e = |e|$ ) of a baryon  $B$  for  $B = B'$ , but zero otherwise. The anomalous magnetic moment is denoted by  $\kappa_{BB'}$  for which we use experimental values listed in the Particle Data Group [22]<sup>2</sup>.

The photon coupling to the pseudoscalar meson current is given by

$$L_{\gamma\pi\pi} = -ie \left[ \pi^- \partial^\mu \pi^+ - (\partial^\mu \pi^-) \pi^+ \right] A_\mu, \quad (\text{B18})$$

$$L_{\gamma KK} = -ie \left[ K^- \partial^\mu K^+ - (\partial^\mu K^-) K^+ \right] A_\mu. \quad (\text{B19})$$

The minimal substitutions ( $\partial_\mu \rightarrow ieA_\mu[Q, ]$ ) to the  $BBMM$  [Eq. (B5)] and  $BBM$  [Eq. (B6)] interactions respectively give

$$\mathcal{L}_{\gamma BBMM} = -\frac{e}{4f^2} \left\langle \bar{B} \gamma^\mu \{ (M [Q, M] - [Q, M] M) B - B (M [Q, M] - [Q, M] M) \} \right\rangle A_\mu, \quad (\text{B20})$$

and

$$\mathcal{L}_{\gamma BBM} = -ie\sqrt{2}g_{PS}^{\text{oct}} \left( \alpha_{PS} \left\langle \bar{B} \gamma_5 \gamma^\mu B [Q, M] \right\rangle_F + (1 - \alpha_{PS}) \left\langle \bar{B} \gamma_5 \gamma^\mu B [Q, M] \right\rangle_D \right) A_\mu, \quad (\text{B21})$$

where  $Q$  is the quark charge matrix  $Q = \text{diag}(2/3, -1/3, -1/3)$ .

The electromagnetic interactions involving the vector mesons are due to the U(1) axial anomaly, and are given by

$$L_{\gamma VM} = g_{VM} \epsilon^{\alpha\beta\gamma\delta} M \partial_\alpha A_\beta \partial_\gamma V_\delta. \quad (\text{B22})$$

The couplings  $g_{VM}$  are determined by experimental  $V \rightarrow \gamma M$  decay widths [22], and the relative phases are fixed by the SU(3) relation. The numerical values for  $g_{VM}$  are given in TABLE II.<sup>3</sup>

<sup>2</sup> The magnetic moment for  $\Sigma^0$  has not been measured, and we use a quark model prediction [22]. We also use the quark model to fix the sign for  $\kappa_{\Lambda\Sigma^0}$ .

<sup>3</sup> Although we find  $|g_{\gamma\phi\pi^0}| = 0.04 \text{ GeV}^{-1}$  from data, the SU(3) predicts it to be zero, and we cannot find its phase. In this work, we set it to be zero.

TABLE II. Coupling constants for  $L_{\gamma VM}$  given in Eq. (B22).

$\gamma VM$	$\gamma K^{*\pm} K^\mp$	$\gamma K^{*0} \bar{K}^0$	$\gamma \bar{K}^{*0} K^0$	$\gamma \omega \eta$	$\gamma \omega \pi^0$	$\gamma \rho^0 \eta$	$\gamma \rho^0 \pi^0$	$\gamma \rho^\pm \pi^\mp$	$\gamma \phi \eta$	$\gamma \phi \pi^0$
$g_{\gamma VM} \text{ (GeV}^{-1}\text{)}$	0.254	-0.388	-0.388	0.169	0.736	0.565	0.234	0.221	0.216	0

### 3. Matrix elements and coupling constants

In this subsection, we evaluate matrix elements of the Lagrangians defined above, in order to introduce a coupling constant for a given set of incoming and outgoing particles. The coupling constants will be used to write down the photoproduction amplitudes in the next section. We will often use an index  $i$  (or  $j$ ) = 1, ..., 10 to specify a pair of meson and baryon,  $M_i B_i = K^- p, \bar{K}^0 n, \pi^0 \Lambda, \pi^0 \Sigma^0, \eta \Lambda, \eta \Sigma^0, \pi^+ \Sigma^-, \pi^- \Sigma^+, K^+ \Xi^-, K^0 \Xi^0$ , respectively. Also we denote four-momenta for  $M_i$  and  $B_i$  as  $k_i$  and  $p_i$ , respectively.

The matrix element of the  $BBMM$  interaction defined in Eq. (B5) is given by

$$\langle B_j(p_j) M_j(k_j) | \mathcal{L}_{BBMM} | B_i(p_i) M_i(k_i) \rangle = \sqrt{\frac{M_{B_i} M_{B_j}}{4E_{B_i} E_{B_j} E_{M_i} E_{M_j}}} \frac{C_{ji}}{4f^2} \bar{u}_{B_j}(p_j) (\not{k}_j + \not{k}_i) u_{B_i}(p_i), \quad (\text{B23})$$

where the energy for a particle  $x$  is denoted by  $E_x(p_x) = \sqrt{\mathbf{p}_x^2 + M_x^2}$  where  $M_x$  is the mass of  $x$ ; the values of  $M_x$  are from Ref. [22]. The couplings  $C_{ji}$  are tabulated in TABLE 1 of Ref. [25]. The matrix element of the  $BBM$  interaction defined in Eq. (B6) is given with a coupling constant  $D_B^j$  as

$$\langle B_j(p_j) M_j(k_j) | \mathcal{L}_{BBM} | B(p) \rangle = i \sqrt{\frac{M_B M_{B_j}}{2E_B E_{B_j} E_{M_j}}} D_B^{M_j B_j} \bar{u}_{B_j}(p_j) \gamma_5 \not{k}_j u_B(p), \quad (\text{B24})$$

with

$$D_B^{M_j B_j} = D_B^j = -\sqrt{2} g_{PS}^{\text{oct}} \langle B_j M_j | \left( \alpha_{PS} \langle \bar{\mathcal{B}} \mathcal{B} \mathcal{M} \rangle_F + (1 - \alpha_{PS}) \langle \bar{\mathcal{B}} \mathcal{B} \mathcal{M} \rangle_D \right) | B \rangle. \quad (\text{B25})$$

Similarly, the matrix elements of the  $VMM$ ,  $BBV$ ,  $BBVM$ , and  $VVM$  interactions defined respectively in Eqs. (B11), (B12), (B15) and (B16) are given below:

$$\langle M(k) M'(k') | \mathcal{L}_{VMM} | V(k_V) \rangle = -g_{VMM'} (k^\mu - k'^\mu) \epsilon_\mu^V \frac{1}{\sqrt{8E_V E_M E_{M'}}}, \quad (\text{B26})$$

where  $\epsilon_\mu^V$  is the polarization vector for the vector meson  $V$ , and

$$\langle B'(p') | \mathcal{L}_{BBV} | B(p) V(k_V) \rangle = -\sqrt{\frac{M_B M_{B'}}{2E_B E_{B'} E_V}} g_{VBB'} \bar{u}_{B'}(p') \left( \gamma_\mu + i \frac{\kappa_{VBB'}}{2M_B} \sigma_{\mu\nu} k_V^\nu \right) \epsilon_\mu^V u_B(p), \quad (\text{B27})$$

$$\langle B_j(p_j) M_j(k_j) | \mathcal{L}_{BBVM} | B(p) V(k_V) \rangle = i \sqrt{\frac{M_B M_{B_j}}{4E_B E_{B_j} E_V E_{M_j}}} g_{V B_j}^{M_j B_j} \bar{u}_{B_j}(p_j) \not{\epsilon}_V \gamma_5 u_B(p) \quad (\text{B28})$$

$$\langle V'(k_{V'}) M(k) | \mathcal{L}_{VVM} | V(k_V) \rangle = g_{V V' M} \epsilon_{\alpha\beta\gamma\delta} k_V^\alpha \epsilon_{V'}^\beta k_V^\gamma \epsilon_V^\delta \frac{1}{\sqrt{8E_V E_{V'} E_M}}, \quad (\text{B29})$$

where we have introduced the coupling constants,  $g_{VMM'}$ ,  $g_{VBB'}$ ,  $\kappa_{VBB'}$ ,  $g_{VB}^{M_j B_j}$  ( $= g_{VB}^j$ ) and  $g_{VV'M}$ , and they are related to the parameters in the original Lagrangians through equations similar to Eq. (B25).

Finally, the tensor couplings for the vector mesons ( $\kappa_{VBB'}$ ) are fixed using the SU(3) relation for the magnetic coupling ( $G_{VBB'}^m = g_{VBB'}(1 + \kappa_{VBB'})$ ), as given by

$$G_{B_1 B_2 V_1}^m = \langle B_2 | \left[ -\sqrt{2} g_m^{\text{oct}} \left( \alpha_V^m \langle \bar{\mathcal{B}} \mathcal{B} \mathcal{V} \rangle_F + (1 - \alpha_V^m) \langle \bar{\mathcal{B}} \mathcal{B} \mathcal{V} \rangle_D \right) - \frac{g_m^{\text{sin}}}{\sqrt{3}} \langle \bar{\mathcal{B}} \mathcal{B} \mathcal{V} \rangle_S \right] | B_1 V_1 \rangle, \quad (\text{B30})$$

where we use  $g_m^{\text{oct}} = -9$ ,  $g_m^{\text{sin}} = -8.82$ , and the static SU(6) value,  $\alpha_V^m = 0.4$ .

### Appendix C: Tree-level photoproduction amplitudes

We present expressions for our tree-level photo-production amplitudes for  $\gamma(q) + p(p) \rightarrow K^+(k) + M_j(k_j) + B_j(p')$  where the four-momentum for each particle is given in the parentheses. The expressions are gauge invariant for  $\mathcal{O}(1)$  and  $\mathcal{O}(1/M_B)$  terms. The final state is specified by the index  $j$  introduced in the previous section. We denote each amplitude by  $V_x^j$  where the label  $x = \mathbf{1(a)}, \mathbf{1(b)}, \dots$  specifies the mechanism by referring to the diagram with the same label in Figs. 1-3. In what follows, kinematical variables (momentum, energy, polarization vector) are understood to be those in the  $M_j B_j$  center-of-mass system, and omit \* that has been used in Eqs. (1) and (2) for simplicity. All coupling constants appearing in the expressions have been defined in Appendix B.

First we introduce building blocks,  $F_1, \dots, F_4$ , to express  $V_x^j$  in a concise manner:

$$F_1 = \frac{M_p}{E_p(p+q)} \frac{1}{q + E_p(p) - E_p(p+q)} \left( \frac{\mathbf{p} + (\mathbf{p} + \mathbf{q})}{2M_p} + i \frac{(1 + \kappa_p)(\boldsymbol{\sigma} \times \mathbf{q})}{2M_p} \right) \cdot \boldsymbol{\epsilon}, \quad (\text{C1})$$

$$F_2 = \left( Q_{B_j} \frac{(\mathbf{p}' - \mathbf{q}) + \mathbf{p}'}{2M_{B_j}} + i \frac{(Q_{B_j} + \kappa_{B_j})(\boldsymbol{\sigma} \times \mathbf{q})}{2M_p} \right) \cdot \boldsymbol{\epsilon} \\ \times \frac{M_{B_j}}{E_{B_j}(p' - q)} \frac{1}{E_p(p) - E_{K^+}(k) - E_{M_j}(k_j) - E_{B_j}(p' - q)}, \quad (\text{C2})$$

$$F_3 = \frac{(\mathbf{k} - (\mathbf{q} - \mathbf{k})) \cdot \boldsymbol{\epsilon}}{(q - k)^2 - M_{K^+}^2}, \quad (\text{C3})$$

$$F_4 = \frac{(\mathbf{k}_j - (\mathbf{q} - \mathbf{k}_j)) \cdot \boldsymbol{\epsilon}}{(q - k_j)^2 - M_{M_j}^2}, \quad (\text{C4})$$

where the electric charge of a particle  $x$  in unit of  $e$  is denoted by  $Q_x$ . The polarization vector of the photon is denoted by  $\boldsymbol{\epsilon}$ . The squared momenta in the denominators of  $F_3$  and  $F_4$  are Lorentz scalar.

#### 1. Gauged Weinberg-Tomozawa terms

With the minimal substitution to the Weinberg-Tomozawa terms, the resulting photo-production amplitudes shown in Fig. 1 are given by the following expressions:

$$V_{1(a)}^j = e \frac{C_{j1}}{4f^2} \left[ (k_j^0 - k^0) + \frac{1}{2M_B} \{ (\mathbf{k} - \mathbf{k}_j)^2 + 2i\mathbf{k} \times \mathbf{k}_j \cdot \boldsymbol{\sigma} \} \right] F_1 - e \frac{C_{j1}}{4f^2} \frac{1}{2M_B} (\mathbf{k}_j - \mathbf{k} + i\boldsymbol{\sigma} \times (\mathbf{k}_j - \mathbf{k})) \cdot \boldsymbol{\epsilon} , \quad (\text{C5})$$

$$V_{1(b)}^j = e \frac{C_{j1}}{4f^2} F_2 \left[ (k_j^0 - k^0) + \frac{1}{2M_B} \{ (\mathbf{k} - \mathbf{k}_j) \cdot (\mathbf{k} - \mathbf{k}_j - 2\mathbf{q}) + 2i\mathbf{k} \times \mathbf{k}_j \cdot \boldsymbol{\sigma} \} \right] - e Q_{B_j} \frac{C_{j1}}{4f^2} \frac{1}{2M_B} (\mathbf{k}_j - \mathbf{k} - i\boldsymbol{\sigma} \times (\mathbf{k}_j - \mathbf{k})) \cdot \boldsymbol{\epsilon} , \quad (\text{C6})$$

$$V_{1(c)}^j = e \frac{C_{j1}}{4f^2} \left[ k_j^0 + k'^0 + \frac{1}{2M_B} \{ (\mathbf{k}' + \mathbf{k}_j)^2 + 2i(\mathbf{k}_j \times \mathbf{k}') \cdot \boldsymbol{\sigma} \} \right] F_3 , \quad (\text{C7})$$

$$V_{1(d)}^j = e Q_{M_j} \frac{C_{j1}}{4f^2} \left[ k^0 + k_j'^0 - \frac{1}{2M_B} \{ (\mathbf{k} - \mathbf{k}_j - \mathbf{q}) \cdot (\mathbf{k} + \mathbf{k}_j') + 2i(\mathbf{k}_j' \times \mathbf{k}) \cdot \boldsymbol{\sigma} \} \right] F_4 , \quad (\text{C8})$$

$$V_{1(e)}^j = -e \frac{C_{j1}}{4f^2} (Q_{M_1} + Q_{M_j}) \frac{1}{2M_B} (\mathbf{k} - \mathbf{q} - \mathbf{k}_j + i\boldsymbol{\sigma} \times (\mathbf{q} - \mathbf{k} - \mathbf{k}_j)) \cdot \boldsymbol{\epsilon} . \quad (\text{C9})$$

The baryon mass  $M_B$  in  $\mathcal{O}(1/M_B)$  terms is set to  $M_B = M_p$  in actual numerical calculation. Momenta for intermediate mesons in Eqs. (C7) and (C8) are  $k' = q - k$ ,  $k_j' = q - k_j$ , respectively. The last terms in Eqs. (C5) and (C6) are, in the time-ordered perturbation, due to the propagation of the anti-baryons. For channels where  $B_j = \Lambda$  or  $\Sigma^0$ , the mechanism of Fig. 1 (b) contains the  $\Lambda$ - $\Sigma^0$  mixing mechanism, and the following term needs to be added to Eq. (C6):

$$V_{1(b)}^j = e \left( i \frac{\kappa_{\Lambda\Sigma^0} (\boldsymbol{\sigma} \times \mathbf{q})}{2M_p} \right) \cdot \boldsymbol{\epsilon} \frac{M_{B_{j'}}}{E_{B_{j'}}(p' - q) E_p(p) - E_{K^+}(k) - E_{M_j}(k_j) - E_{B_{j'}}(p' - q)} \frac{1}{2M_B} \times \frac{C_{j1}}{4f^2} \left[ (k_j^0 - k^0) + \frac{1}{2M_B} \{ (\mathbf{k} - \mathbf{k}_j) \cdot (\mathbf{k} - \mathbf{k}_j - 2\mathbf{q}) + 2i\mathbf{k} \times \mathbf{k}_j \cdot \boldsymbol{\sigma} \} \right] , \quad (\text{C10})$$

where we have used a channel index  $j'$  to indicate  $B_{j'} = \Lambda(\Sigma^0)$  for  $B_j = \Sigma^0(\Lambda)$  and  $M_{j'} = M_j$ .

## 2. Gauged Born terms

For convenience, we introduce some building blocks as follows:

$$O_1 = \boldsymbol{\sigma} \cdot \mathbf{k}_j \left( 1 + \frac{k_j^0}{2M_B} \right) , \quad (\text{C11})$$

$$O_2 = \boldsymbol{\sigma} \cdot \mathbf{k} \left( 1 - \frac{k^0}{2M_B} \right) + \frac{k^0}{M_B} \boldsymbol{\sigma} \cdot \mathbf{q} , \quad (\text{C12})$$

$$O_3 = \boldsymbol{\sigma} \cdot \mathbf{k} \left( 1 - \frac{k^0}{2M_B} \right) + \frac{k^0}{M_B} \boldsymbol{\sigma} \cdot \mathbf{k}_j , \quad (\text{C13})$$

$$O_4 = \boldsymbol{\sigma} \cdot \mathbf{k}_j \left( 1 + \frac{k_j^0}{2M_B} \right) - \frac{k_j^0}{M_B} \boldsymbol{\sigma} \cdot (\mathbf{k} - \mathbf{q}) , \quad (\text{C14})$$

$$S_1^{Y^0} = \frac{1}{q + E_p(p) - E_{K^+}(k) - \tilde{M}_{Y^0}} , \quad (\text{C15})$$



$$S_2^{Y^0} = \frac{M_{Y^0}}{E_{Y^0}(p-k)} \frac{1}{E_p(p) - E_{K^+}(k) - E_{Y^0}(p-k)} , \quad (\text{C16})$$

$$S_3^{B_x} = \frac{M_{B_x}}{E_{B_x}(p+q-k_j)} \frac{1}{q + E_p(p) - E_{M_j}(k_j) - E_{B_x}(p+q-k_j)} , \quad (\text{C17})$$

$$S_4^{B_x} = \frac{M_{B_x}}{E_{B_x}(p-k_j)} \frac{1}{E_p(p) - E_{M_j}(k_j) - E_{B_x}(p-k_j)} , \quad (\text{C18})$$

where  $Y^0$  is either  $\Lambda$  or  $\Sigma^0$ . The quantity  $\tilde{M}_{Y^0}$  is a 'bare' mass, and we use it only in  $S_1^{Y^0}$ . The  $p$ -wave rescattering following  $S_1^{Y^0}$  renormalize the bare mass to give the physical mass. Because we use the  $p$ -wave scattering amplitude from Ref. [21], we also use the bare mass from Ref. [21];  $\tilde{M}_\Lambda = 1078$  MeV and  $\tilde{M}_{\Sigma^0} = 1104$  MeV. With the minimal substitution to the Born terms, the resulting photo-production amplitudes shown in Fig. 2 are given by the following expressions:

$$V_{2(a)}^j = e \sum_{Y^0} D_{Y^0}^j D_{Y^0}^1 S_1^{Y^0} \left[ \left( 1 - \frac{k^0}{2M_B} \right) O_1 \boldsymbol{\sigma} \cdot \mathbf{k} F_1 + \frac{k^0}{2M_B} \boldsymbol{\sigma} \cdot \mathbf{k}_j \boldsymbol{\sigma} \cdot \boldsymbol{\epsilon} \right] , \quad (\text{C19})$$

$$V_{2(b)}^j = e \sum_{Y^0} D_{Y^0}^j D_{Y^0}^1 S_1^{Y^0} O_1 \boldsymbol{\sigma} \cdot \boldsymbol{\epsilon} , \quad (\text{C20})$$

$$V_{2(c)}^j = -e \sum_{Y^0} D_{Y^0}^j D_{Y^0}^1 S_1^{Y^0} \left( 1 + \frac{k^0}{2M_B} \right) O_1 \boldsymbol{\sigma} \cdot \mathbf{k}' F_3 , \quad (\text{C21})$$

$$V_{2(d)}^j = e \sum_{Y^0} D_{Y^0}^j S_1^{Y^0} \left[ D_{Y^0}^1 \kappa_{Y^0} S_2^{Y^0} + \sum_{Y^{0'} \neq Y^0} D_{Y^{0'}}^1 \kappa_{\Lambda \Sigma^0} S_2^{Y^{0'}} \right] O_1 i \frac{\boldsymbol{\sigma} \times \mathbf{q} \cdot \boldsymbol{\epsilon}}{2M_p} O_2 , \quad (\text{C22})$$

$$V_{2(e)}^j = e Q_{M_j} \sum_{Y^0} D_{Y^0}^j D_{Y^0}^1 S_2^{Y^0} \boldsymbol{\sigma} \cdot \boldsymbol{\epsilon} O_2 , \quad (\text{C23})$$

$$V_{2(f)}^j = -e Q_{M_j} \sum_{Y^0} D_{Y^0}^j D_{Y^0}^1 S_2^{Y^0} F_4 \left\{ \boldsymbol{\sigma} \cdot \mathbf{k}'_j + \frac{k_j^0}{2M_B} \boldsymbol{\sigma} \cdot (\mathbf{k}_j + \mathbf{q}) \right\} O_2 , \quad (\text{C24})$$

$$V_{2(g)}^j = e \sum_{Y^0} D_{Y^0}^j D_{Y^0}^1 S_2^{Y^0} F_2 \left\{ \left( 1 + \frac{k_j^0}{2M_B} \right) \boldsymbol{\sigma} \cdot \mathbf{k}_j + \frac{k_j^0}{M_B} \boldsymbol{\sigma} \cdot \mathbf{q} \right\} O_2 \\ - e Q_{B_j} \sum_{Y^0} D_{Y^0}^j D_{Y^0}^1 S_2^{Y^0} \frac{k_j^0}{2M_B} \boldsymbol{\sigma} \cdot \boldsymbol{\epsilon} \boldsymbol{\sigma} \cdot \mathbf{k} , \quad (\text{C25})$$

$$V_{2(h)}^j = e \sum_{B_x} D_{B_x}^{K^+ B_j} D_{B_x}^{M_j p} S_3^{B_x} O_3 \left\{ \left( 1 + \frac{k_j^0}{2M_B} \right) \boldsymbol{\sigma} \cdot \mathbf{k}_j - \frac{k_j^0}{M_B} \boldsymbol{\sigma} \cdot \mathbf{k} \right\} F_1 \\ - e \sum_{B_x} D_{B_x}^{K^+ B_j} D_{B_x}^{M_j p} S_3^{B_x} \frac{k_j^0}{2M_B} \boldsymbol{\sigma} \cdot \mathbf{k} \boldsymbol{\sigma} \cdot \boldsymbol{\epsilon} , \quad (\text{C26})$$

$$V_{2(i)}^j = e Q_{M_j} \sum_{B_x} D_{B_x}^{K^+ B_j} D_{B_x}^{M_j p} S_3^{B_x} O_3 \boldsymbol{\sigma} \cdot \boldsymbol{\epsilon} , \quad (\text{C27})$$

$$V_{2(j)}^j = -e Q_{M_j} \sum_{B_x} D_{B_x}^{K^+ B_j} D_{B_x}^{M_j p} S_3^{B_x} O_3 \left\{ \left( 1 - \frac{k_j^0}{2M_B} \right) \boldsymbol{\sigma} \cdot \mathbf{k}'_j - \frac{k_j^0}{M_B} \boldsymbol{\sigma} \cdot (\mathbf{k} - \mathbf{q}) \right\} F_4 , \quad (\text{C28})$$

$$V_{2(k)}^j = e \sum_{B_x} D_{B_x}^{K^+ B_j} D_{B_x}^{M_j p} S_3^{B_x} O_3 \left( Q_{B_x} \frac{(\mathbf{k} - \mathbf{k}_j - \mathbf{q}) + (\mathbf{k} - \mathbf{k}_j)}{2M_{B_x}} + i \frac{(Q_{B_x} + \kappa_{B_x}) \boldsymbol{\sigma} \times \mathbf{q}}{2M_p} \right) \cdot \boldsymbol{\epsilon} S_4^{B_x} O_4$$

$$-e \sum_{B_x} Q_{B_x} D_{B_x}^{K^+ B_j} D_{B_x}^{M_j p} \left[ S_3^{B_x} \frac{k_j^0}{2M_B} \boldsymbol{\sigma} \cdot \mathbf{k} \boldsymbol{\sigma} \cdot \boldsymbol{\epsilon} + S_4^{B_x} \frac{k^0}{2M_B} \boldsymbol{\sigma} \cdot \boldsymbol{\epsilon} \boldsymbol{\sigma} \cdot \mathbf{k}_j \right], \quad (\text{C29})$$

$$V_{2(l)}^j = e \sum_{B_x} D_{B_x}^{K^+ B_j} D_{B_x}^{M_j p} S_4^{B_x} \boldsymbol{\sigma} \cdot \boldsymbol{\epsilon} O_4, \quad (\text{C30})$$

$$V_{2(m)}^j = -e \sum_{B_x} D_{B_x}^{K^+ B_j} D_{B_x}^{M_j p} S_4^{B_x} F_3 \left\{ \left( 1 + \frac{k'^0}{2M_B} \right) \boldsymbol{\sigma} \cdot \mathbf{k}' + \frac{k'^0}{M_B} \boldsymbol{\sigma} \cdot \mathbf{k}_j \right\} O_4, \quad (\text{C31})$$

$$V_{2(n)}^j = e \sum_{B_x} D_{B_x}^{K^+ B_j} D_{B_x}^{M_j p} S_4^{B_x} F_2 \left\{ \left( 1 - \frac{k^0}{2M_B} \right) \boldsymbol{\sigma} \cdot \mathbf{k} + \frac{k^0}{M_B} \boldsymbol{\sigma} \cdot (\mathbf{q} + \mathbf{k}_j) \right\} O_4$$

$$-e Q_{B_j} \sum_{B_x} D_{B_x}^{K^+ B_j} D_{B_x}^{M_j p} S_4^{B_x} \frac{k^0}{2M_B} \boldsymbol{\sigma} \cdot \boldsymbol{\epsilon} \boldsymbol{\sigma} \cdot \mathbf{k}_j, \quad (\text{C32})$$

where the summation  $\sum_{B_x}$  runs over the octet baryons contained in Eq. (B4). We do not consider  $\Lambda$ - $\Sigma^0$  mixing mechanism due to the anomalous magnetic moment in Eqs. (C29) and (C32) because (i) it contributes to unimportant  $K^+ \Xi^-$  channel in Eq. (C29); (ii) contribution of Eq. (C32) is rather small.

### 3. Vector meson exchange terms

We introduce some building blocks as follows to construct  $V_x^j$  in this subsection:

$$O_5(a) = (a^0 \mathbf{q} \cdot (\mathbf{q} - \mathbf{a}) - q^0 \mathbf{a} \cdot (\mathbf{q} - \mathbf{a})) \boldsymbol{\sigma} \cdot \boldsymbol{\epsilon} + (q^0 \boldsymbol{\sigma} \cdot \mathbf{a} - a^0 \boldsymbol{\sigma} \cdot \mathbf{q}) (\mathbf{q} - \mathbf{a}) \cdot \boldsymbol{\epsilon}, \quad (\text{C33})$$

$$O_6(a) = i (q^0 \boldsymbol{\sigma} \times \mathbf{a} - a^0 \boldsymbol{\sigma} \times \mathbf{q}) \cdot \boldsymbol{\epsilon}, \quad (\text{C34})$$

$$O_7 = \left\{ \boldsymbol{\sigma} \cdot (\mathbf{q} - \mathbf{k} - \mathbf{k}_j) - \frac{q^0 - k^0 - k_j^0}{2M_B} \boldsymbol{\sigma} \cdot (\mathbf{k} - \mathbf{q} - \mathbf{k}_j) \right\}$$

$$\times i (q^0 \mathbf{k} \times \mathbf{k}_j + k^0 \mathbf{k}_j \times \mathbf{q} + k_j^0 \mathbf{q} \times \mathbf{k}) \cdot \boldsymbol{\epsilon}, \quad (\text{C35})$$

where  $a$  is a four-vector. We also define the following propagators:

$$S_5^{K^*} = \frac{1}{(q - k)^2 - M_{K^*}^2 + iM_{K^*} \Gamma_{K^*}}, \quad (\text{C36})$$

$$S_6^X = \frac{1}{(q - k - k_j)^2 - M_X^2 + iM_X \Gamma_X}, \quad (\text{C37})$$

$$S_7^V = \frac{1}{(q - k_j)^2 - M_V^2 + iM_V \Gamma_V}, \quad (\text{C38})$$

$$S_8^V = \frac{1}{(k + k_j)^2 - M_V^2 + iM_V \Gamma_V}, \quad (\text{C39})$$

where  $X$  is a vector or pseudoscalar meson, and  $V$  is a vector meson. The mass of a particle  $X$  is denoted by  $M_X$ , and its width by  $\Gamma_X$  for which we use the values from the PDG [22]. For pseudoscalar particles, the width is set to zero. We also define

$$\mathbf{J}_B = \frac{\mathbf{p} + \mathbf{p}'}{2M_B} + i \frac{(1 + \kappa_{VpB_j}) \boldsymbol{\sigma} \times (\mathbf{p}' - \mathbf{p})}{2M_B}, \quad (\text{C40})$$

$$J_1^0 = \mathbf{k}_j \times (\mathbf{k} - \mathbf{q}) \cdot \mathbf{J}_B, \quad (\text{C41})$$

$$\mathbf{J}_1 = \mathbf{k}_j \times (\mathbf{k} - \mathbf{q}) + k_j^0 (\mathbf{k} - \mathbf{q}) \times \mathbf{J}_B + (q^0 - k^0) \mathbf{k}_j \times \mathbf{J}_B, \quad (\text{C42})$$

$$\mathbf{J}_2^0 = \mathbf{k} \times (\mathbf{k}_j - \mathbf{q}) \cdot \mathbf{J}_B, \quad (\text{C43})$$

$$\mathbf{J}_2 = \mathbf{k} \times (\mathbf{k}_j - \mathbf{q}) + k^0 (\mathbf{k}_j - \mathbf{q}) \times \mathbf{J}_B + (q^0 - k_j^0) \mathbf{k} \times \mathbf{J}_B. \quad (\text{C44})$$

Thus, the photo-production amplitudes due to vector meson exchanges shown in Fig. 3 are given by the following expressions:

$$\begin{aligned} V_{3(a)}^j &= g_{\gamma K^*-K^+} \sum_{Y^0} g_{K^*-pY^0} D_{Y^0}^j S_1^{Y^0} S_5^{K^*} O_1 \left\{ \left( 1 + \frac{k^0}{2M_B} \right) i\mathbf{q} \times \mathbf{k} \cdot \boldsymbol{\epsilon} + \frac{1 + \kappa_{K^*-pY^0}}{2M_B} O_5(k) \right\} \\ &\quad + g_{\gamma K^*-K^+} \sum_{Y^0} g_{K^*-pY^0} D_{Y^0}^j S_5^{K^*} \frac{k_j^0}{2M_B} O_6(k), \end{aligned} \quad (\text{C45})$$

$$V_{3(b)}^j = ig_{\gamma K^*-K^+} g_{K^*-p}^j S_5^{K^*} \left\{ k^0 \boldsymbol{\sigma} \times \mathbf{q} - q^0 \boldsymbol{\sigma} \times \mathbf{k} + \frac{\boldsymbol{\sigma} \cdot (\mathbf{k} - \mathbf{q} - \mathbf{k}_j)}{2M_B} \mathbf{q} \times \mathbf{k} \right\} \cdot \boldsymbol{\epsilon}, \quad (\text{C46})$$

$$\begin{aligned} V_{3(c)}^j &= g_{\gamma K^*-K^+} \sum_{B_x} g_{K^*-B_x B_j} D_p^{M_j B_x} S_4^{B_x} S_5^{K^*} \\ &\quad \times \left[ \left\{ \left( 1 + \frac{q^0 - k^0}{2M_B} \right) i\mathbf{q} \times \mathbf{k} + \frac{q^0}{M_B} i\mathbf{k}_j \times \mathbf{k} - \frac{k^0}{M_B} i\mathbf{k}_j \times \mathbf{q} \right\} \cdot \boldsymbol{\epsilon} + \frac{1 + \kappa_{K^*-B_x B_j}}{2M_B} O_5(k) \right] O_4 \\ &\quad + g_{\gamma K^*-K^+} \sum_{B_x} g_{K^*-B_x B_j} D_p^{M_j B_x} S_5^{K^*} \frac{k_j^0}{2M_B} O_6(k), \end{aligned} \quad (\text{C47})$$

$$V_{3(d)}^j = -2 g_{\gamma K^*-K^+} \sum_{M_x} g_{K^*-M_x M_j} D_{B_j}^{M_x p} S_5^{K^*} S_6^{M_x} O_7, \quad (\text{C48})$$

$$\begin{aligned} V_{3(e)}^j &= \sum_{V, B_x} g_{\gamma V M_j} g_{V p B_x} D_{B_x}^{K^+ B_j} S_3^{B_x} S_7^V O_3 \\ &\quad \times \left[ \left\{ \left( 1 + \frac{q^0 + k_j^0}{2M_B} \right) i\mathbf{q} \times \mathbf{k}_j + \frac{q^0}{M_B} i\mathbf{k}_j \times \mathbf{k} + \frac{k_j^0}{M_B} i\mathbf{k} \times \mathbf{q} \right\} \cdot \boldsymbol{\epsilon} + \frac{1 + \kappa_{V p B_x}}{2M_B} O_5(k_j) \right] \\ &\quad + \sum_{V, B_x} g_{\gamma V M_j} g_{V p B_x} D_{B_x}^{K^+ B_j} S_7^V \frac{k^0}{2M_B} O_6(k_j), \end{aligned} \quad (\text{C49})$$

$$V_{3(f)}^j = i \sum_V g_{\gamma V M_j} g_{V p}^{K^+ B_j} S_7^V \left\{ k_j^0 \boldsymbol{\sigma} \times \mathbf{q} - q^0 \boldsymbol{\sigma} \times \mathbf{k}_j + \frac{\boldsymbol{\sigma} \cdot (\mathbf{k} - \mathbf{q} - \mathbf{k}_j)}{2M_B} \mathbf{q} \times \mathbf{k}_j \right\} \cdot \boldsymbol{\epsilon}, \quad (\text{C50})$$

$$\begin{aligned} V_{3(g)}^j &= \sum_{V, Y^0} g_{\gamma V M_j} g_{V Y^0 B_j} D_p^{K^+ Y^0} S_2^{Y^0} S_7^V \left\{ \left( 1 + \frac{q^0 + k_j^0}{2M_B} \right) i\mathbf{q} \times \mathbf{k}_j \cdot \boldsymbol{\epsilon} + \frac{1 + \kappa_{V Y^0 B_j}}{2M_B} O_5(k_j) \right\} O_2 \\ &\quad + \sum_{V, Y^0} g_{\gamma V M_j} g_{V Y^0 B_j} D_p^{K^+ Y^0} S_7^V \frac{k^0}{2M_B} O_6(k_j), \end{aligned} \quad (\text{C51})$$

$$V_{3(h)}^j = 2 \sum_{V, M_x} g_{\gamma V M_j} g_{V M_x K^+} D_{B_j}^{M_x p} S_7^V S_6^{M_x} O_7, \quad (\text{C52})$$

$$V_{3(i)}^j = -2 \sum_{V, M_x} g_{\gamma V M_x} g_{V K^+ M_j} D_{B_j}^{M_x p} S_8^V S_6^{M_x} O_7, \quad (\text{C53})$$

$$V_{3(j)}^j = g_{\gamma K^*-K^+} \sum_{V_x} g_{K^*-V_x M_j} g_{V_x p B_j} S_5^{K^*} S_6^{V_x} \left( -q^0 \mathbf{k} \times \mathbf{J}_1 + k^0 \mathbf{q} \times \mathbf{J}_1 + J_1^0 \mathbf{k} \times \mathbf{q} \right) \cdot \boldsymbol{\epsilon}, \quad (\text{C54})$$

$$V_{3(k)}^j = \sum_{V, V_x} g_{\gamma V M_j} g_{V V_x K^+} g_{V_x p B_j} S_7^V S_6^{V_x} \left( -q^0 \mathbf{k}_j \times \mathbf{J}_2 + k_j^0 \mathbf{q} \times \mathbf{J}_2 + J_2^0 \mathbf{k}_j \times \mathbf{q} \right) \cdot \boldsymbol{\epsilon}. \quad (\text{C55})$$

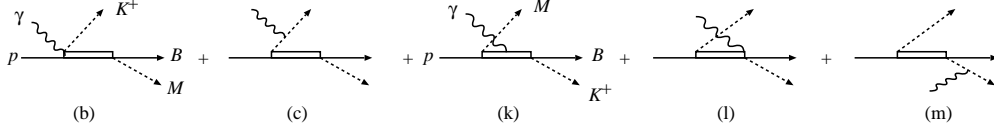


FIG. 11. Nucleon (hyperon) resonance exchange diagrams. The diagrams (b), (c), (k), (l), and (m) are obtained from Figs. 2 (b), (c), (k), (l), and (m), respectively, by replacing the intermediate nucleons (hyperons) with nucleon (hyperon) resonances of  $J^P = 1/2^+$ .

#### 4. Contact terms

We present expressions for contact terms for  $\gamma + p \rightarrow K^+ + M_j + B_j$ .

$$V_{c1}^j = \lambda_1^j \left( \boldsymbol{\sigma} \cdot \mathbf{k}_j \boldsymbol{\sigma} \cdot \boldsymbol{\epsilon} - \boldsymbol{\sigma} \cdot \mathbf{k}_j \boldsymbol{\sigma} \cdot \mathbf{q} \frac{(2\mathbf{k} - \mathbf{q}) \cdot \boldsymbol{\epsilon}}{(k - q)^2 - M_{K^+}^2} \right), \quad (\text{C56})$$

$$V_{c2}^j = \lambda_2^j \left( \boldsymbol{\sigma} \cdot \boldsymbol{\epsilon} \boldsymbol{\sigma} \cdot \mathbf{k}_j - \boldsymbol{\sigma} \cdot \mathbf{q} \boldsymbol{\sigma} \cdot \mathbf{k}_j \frac{(2\mathbf{k} - \mathbf{q}) \cdot \boldsymbol{\epsilon}}{(k - q)^2 - M_{K^+}^2} \right), \quad (\text{C57})$$

$$V_{c3}^j = \lambda_3^j i(\boldsymbol{\sigma} \times \mathbf{q}) \cdot \boldsymbol{\epsilon}, \quad (\text{C58})$$

where  $\lambda_n^j$  ( $n = 1, 2, 3$ ) are complex coupling constants that depend on the total energy of the whole system. Each term in Eqs. (C56)-(C58) is gauge invariant at  $\mathcal{O}((1/M_B)^0)$ . A microscopic origin of the  $V_{c1}^j$  term can be represented by diagrams shown in Figs. 11 (b) and (c) where a hyperon resonance,  $\Lambda^*$  or  $\Sigma^{0*}$ , of  $J^P = 1/2^+$  ( $J$ :spin,  $P$ :parity) is exchanged. The corresponding expression is given, retaining  $\mathcal{O}((1/M_B)^0)$  terms, as

$$V_{11(b)+11(c)}^j = \sum_{Y^*} C_{11(b)+11(c)}^{Y^*} \frac{\boldsymbol{\sigma} \cdot \mathbf{k}_j \boldsymbol{\sigma} \cdot \boldsymbol{\epsilon} - \boldsymbol{\sigma} \cdot \mathbf{k}_j \boldsymbol{\sigma} \cdot \mathbf{k}' \frac{(2\mathbf{k} - \mathbf{q}) \cdot \boldsymbol{\epsilon}}{(k - q)^2 - M_{K^+}^2}}{q + E_p(p) - E_{K^+}(k) - M_{Y^*} + i\Gamma_{Y^*}/2}, \quad (\text{C59})$$

where  $M_{Y^*}$  and  $\Gamma_{Y^*}$  are the mass and width of the exchanged hyperon resonance, respectively. The constant  $C_{11(b)+11(c)}^{Y^*}$  is the product of coupling constants of  $K^+pY^*$ ,  $MBY^*$  and  $e$  (electric charge). We can derive Eq. (C56) by putting the denominator and coupling together into the  $W$ -dependent complex coupling  $\lambda_1^j$ . Equation (C57) can be derived in a similar way from the diagrams of Figs. 11 (l) and (m), and Eq. (C58) from Figs. 11 (k); for the latter, only the gauge-invariant piece, a term proportional to  $i(\boldsymbol{\sigma} \times \mathbf{q}) \cdot \boldsymbol{\epsilon}$ , is retained. Even though the contact terms of Eqs. (C56)-(C58) can be related to the microscopic mechanisms shown in Fig. 11, by fitting data, they also effectively simulate other mechanisms not explicitly considered in our model.

#### Appendix D: Fitting parameters

We present numerical values for parameters obtained from fitting the data. For the model in which the chiral unitary amplitudes are implemented, they are shown in TABLE III-IV. Also, the cutoff value for the form factor of Eq. (6) obtained from the fit is  $\Lambda = 511$  MeV.

For the model in which the Brit-Wigner amplitudes (Eq. (8)) are implemented, the determined parameters are presented in TABLE V-VII. Also, the cutoff value for the form factor of Eq. (6) is  $\Lambda = 560$  MeV.

TABLE III. The subtraction constants,  $a_{\alpha'}^j(\mu)$  ( $\alpha'=A,B,\dots,K$ ), defined in Eq. (5) for the chiral-unitary-based model. The index  $\alpha'$  has been introduced in TABLE I. While the quoted values are from the chiral unitary model and are fixed, the others are determined by fitting the data.

$j$	A	B	C	D	E	F	G	H	I	J	K
$\bar{K}N$	“-1.84”	-0.49	1.38	1.52	-0.83	1.23	-2.12	-1.66	0.39	-0.06	1.58
$\pi\Sigma$	“-2.00”	1.44	1.39	-1.69	-0.99	0.56	-1.05	-1.55	-2.52	-0.80	-0.36

TABLE IV. Coupling constants,  $\lambda_n^j$  ( $n = 1, 2, 3$ ), defined in Eqs. (C56)-(C58) for the chiral-unitary-based model. They are determined by fitting the data at each value of the total energy  $W$ .

$j$	$W=2.0$ GeV			$W=2.1$ GeV		
	$\lambda_1^j$	$\lambda_2^j$	$\lambda_3^j$	$\lambda_1^j$	$\lambda_2^j$	$\lambda_3^j$
$K^-p$	18.6 +18.6 <i>i</i>	90.7 +49.4 <i>i</i>	1.1 -0.1 <i>i</i>	7.5 +17.5 <i>i</i>	2.2 +7.3 <i>i</i>	1.1 -0.0 <i>i</i>
$\bar{K}^0n$	6.2 +55.9 <i>i</i>	85.7 +177.9 <i>i</i>	0.2 +0.7 <i>i</i>	1.7 +6.2 <i>i</i>	-3.1 +5.9 <i>i</i>	-0.1 +0.3 <i>i</i>
$\pi^0\Sigma^0$	3.4 +0.8 <i>i</i>	0.4 +0.0 <i>i</i>	0.0 +0.7 <i>i</i>	-0.2 -4.4 <i>i</i>	0.6 -1.0 <i>i</i>	0.1 +0.2 <i>i</i>
$\pi^+\Sigma^-$	0.2 +1.5 <i>i</i>	0.4 -0.1 <i>i</i>	0.7 -0.0 <i>i</i>	-1.3 -0.7 <i>i</i>	0.1 +0.0 <i>i</i>	0.5 +0.4 <i>i</i>
$\pi^-\Sigma^+$	9.3 +0.5 <i>i</i>	3.4 +0.1 <i>i</i>	0.1 +0.2 <i>i</i>	1.2 -4.7 <i>i</i>	2.3 +0.4 <i>i</i>	0.2 +0.2 <i>i</i>

$j$	$W=2.2$ GeV			$W=2.3$ GeV		
	$\lambda_1^j$	$\lambda_2^j$	$\lambda_3^j$	$\lambda_1^j$	$\lambda_2^j$	$\lambda_3^j$
$K^-p$	10.7 +12.1 <i>i</i>	-1.5 -5.6 <i>i</i>	0.5 +0.1 <i>i</i>	7.3 +4.4 <i>i</i>	-51.4 -52.4 <i>i</i>	0.5 +0.2 <i>i</i>
$\bar{K}^0n$	3.2 +12.8 <i>i</i>	19.4 +57.4 <i>i</i>	0.9 +0.2 <i>i</i>	-1.8 +4.3 <i>i</i>	1.2 +66.7 <i>i</i>	0.0 -0.1 <i>i</i>
$\pi^0\Sigma^0$	-1.7 -1.9 <i>i</i>	-1.7 +0.5 <i>i</i>	0.3 +0.1 <i>i</i>	-0.5 -2.5 <i>i</i>	1.0 -0.4 <i>i</i>	0.2 -0.1 <i>i</i>
$\pi^+\Sigma^-$	-1.1 +0.2 <i>i</i>	-0.0 +0.0 <i>i</i>	0.4 -0.3 <i>i</i>	-1.9 +0.7 <i>i</i>	0.0 -0.1 <i>i</i>	0.0 +0.4 <i>i</i>
$\pi^-\Sigma^+$	4.3 -3.9 <i>i</i>	1.1 +0.5 <i>i</i>	0.1 +0.0 <i>i</i>	1.6 -3.5 <i>i</i>	1.3 +1.9 <i>i</i>	0.1 +0.2 <i>i</i>

A few notes are in order: The subtraction constants for channels other than  $\bar{K}N$  and  $\pi\Sigma$  are set to the values used in chiral unitary amplitudes; The subtraction constants in the chiral unitary amplitudes are not adjusted in the fit; the contact terms of Eqs. (C56)-(C58) couple to  $\bar{K}N$  and  $\pi\Sigma$  channels only.

- 
- [1] D.W. Thomas, A. Engler, H.E. Fisk, and R.W. Kraemer, Nucl. Phys. **B56**, 15 (1973).
  - [2] R. J. Hemingway, Nucl. Phys. **B253**, 742 (1985).
  - [3] O. Braun *et al.*, Nucl. Phys. **B129**, 1 (1977).
  - [4] S. Prakhov *et al.* [Crystal Ball Collaboration], Phys. Rev. C **70**, 034605 (2004).
  - [5] I. Zychor, M. Buscher, M. Hartmann, A. Kacharava, I. Keshelashvili, A. Khoukaz, V. Kleber and V. Koptev *et al.*, Phys. Lett. B **660**, 167 (2008).
  - [6] J. K. Ahn [LEPS Collaboration], Nucl. Phys. A **721**, 715 (2003).
  - [7] M. Niiyama, H. Fujimura, D. S. Ahn, J. K. Ahn, S. Ajimura, H. C. Bhang, T. H. Chang and

TABLE V. The Breit-Wigner parameters defined in Eq. (8).

$M_{BW}$ (MeV)	$\Gamma_{BW}$ (MeV)	$C_{\bar{K}N,\bar{K}N}^{BW}$	$C_{\bar{K}N,\pi\Sigma}^{BW}$	$C_{\pi\Sigma,\pi\Sigma}^{BW}$
1412.0	67.0	7.54+3.00 <i>i</i>	1.61+0.49 <i>i</i>	0.55−1.66 <i>i</i>

TABLE VI. The subtraction constants,  $a_{\alpha'}^j(\mu)$  ( $\alpha'=A,B,\dots,K.$ ), defined in Eq. (5) for the Breit-Wigner model.

$j$	A	B	C	D	E	F	G	H	I	J	K
$\bar{K}N$	“−1.84”	−0.72	−1.33	2.59	−0.21	1.79	−1.68	−1.66	0.31	−1.82	1.59
$\pi\Sigma$	“−2.00”	0.66	−2.47	−1.35	3.00	0.84	−0.81	−2.76	−2.85	−0.10	−1.53

W. C. Chang *et al.*, Phys. Rev. C **78**, 035202 (2008).

- [8] K. Moriya *et al.* [CLAS Collaboration], Phys. Rev. C **87**, 035206 (2013).
- [9] K. Moriya *et al.* [CLAS Collaboration], Phys. Rev. C **88**, 045201 (2013).
- [10] H. Y. Lu *et al.* [CLAS Collaboration], Phys. Rev. C **88**, 045202 (2013).
- [11] As a recent review on the application of the chiral unitary approach to  $\Lambda(1405)$ , T. Hyodo and D. Jido, Prog. Part. Nucl. Phys. **67**, 55 (2012).
- [12] D. Jido, J. A. Oller, E. Oset, A. Ramos and U. G. Meissner, Nucl. Phys. A **725**, 181 (2003).
- [13] T. Hyodo and W. Weise, Phys. Rev. **C77**, 035204 (2008).
- [14] D. Jido, E. Oset and T. Sekihara, Eur. Phys. J. A **42**, 257 (2009).
- [15] L. Roca and E. Oset, Phys. Rev. C **87**, 055201 (2013).
- [16] L. Roca and E. Oset, arXiv:1307.5752.
- [17] J.C. Nacher, E. Oset, H. Toki, and A. Ramos Phys. Lett. **B455**, 55 (1999).
- [18] J. C. Nacher, E. Oset, H. Toki and A. Ramos, Phys. Lett. B **461**, 299 (1999).
- [19] B. Borasoy, P. C. Bruns, U. -G. Meissner and R. Nissler, Eur. Phys. J. A **34**, 161 (2007).
- [20] E. Oset, A. Ramos, and C. Bennhold, Phys. Lett. **B527**, 99 (2002).
- [21] D. Jido, E. Oset, and A. Ramos, Phys. Rev. C **66**, 055203 (2002).
- [22] J. Beringer *et al.* (Particle Data Group), Phys. Rev. D **86**, 010001 (2012).
- [23] B. C. Pearce and B. Jennings, Nucl. Phys. **A528**, 655 (1991); T. Sato and T.S.H. Lee, Phys. Rev. C **54**, 2660 (1996).
- [24] M. Bando, T. Kugo, K. Yamawaki, Phys. Rep. **164**, 217 (1988).
- [25] E. Oset, and A. Ramos, Nucl. Phys. **A635**, 99 (1998).



TABLE VII. Coupling constants,  $\lambda_n^j$  ( $n = 1, 2, 3$ ), defined in Eqs. (C56)-(C58) for the Breit-Wigner model.

$j$	$W=2.0$ GeV			$W=2.1$ GeV		
	$\lambda_1^j$	$\lambda_2^j$	$\lambda_3^j$	$\lambda_1^j$	$\lambda_2^j$	$\lambda_3^j$
$K^-p$	84.1 +12.6 <i>i</i>	235.8 +56.9 <i>i</i>	1.4 -0.8 <i>i</i>	62.8 +2.6 <i>i</i>	67.2 +61.5 <i>i</i>	1.9 -1.7 <i>i</i>
$\bar{K}^0n$	2.9 +6.6 <i>i</i>	13.5 +6.4 <i>i</i>	0.5 +0.5 <i>i</i>	0.7 +19.1 <i>i</i>	32.1 +16.4 <i>i</i>	-1.6 +1.2 <i>i</i>
$\pi^0\Sigma^0$	0.8 -0.1 <i>i</i>	0.5 -0.1 <i>i</i>	0.2 -0.6 <i>i</i>	-0.4 -2.5 <i>i</i>	1.8 -0.2 <i>i</i>	0.3 -0.3 <i>i</i>
$\pi^+\Sigma^-$	-1.6 +0.3 <i>i</i>	0.4 +0.0 <i>i</i>	0.3 -0.1 <i>i</i>	-1.4 -0.7 <i>i</i>	0.0 -0.2 <i>i</i>	-0.0 -0.2 <i>i</i>
$\pi^-\Sigma^+$	6.1 +0.1 <i>i</i>	3.2 +0.3 <i>i</i>	-0.2 -0.1 <i>i</i>	-0.1 -1.1 <i>i</i>	2.0 -0.4 <i>i</i>	-0.1 +0.5 <i>i</i>

$j$	$W=2.2$ GeV			$W=2.3$ GeV		
	$\lambda_1^j$	$\lambda_2^j$	$\lambda_3^j$	$\lambda_1^j$	$\lambda_2^j$	$\lambda_3^j$
$K^-p$	27.5 +6.1 <i>i</i>	-1.1 +32.2 <i>i</i>	0.3 -0.7 <i>i</i>	0.9 +4.3 <i>i</i>	48.0 +71.6 <i>i</i>	-0.9 -1.0 <i>i</i>
$\bar{K}^0n$	-7.1 -0.1 <i>i</i>	16.2 +6.9 <i>i</i>	-0.1 +0.3 <i>i</i>	6.2 +9.6 <i>i</i>	17.3 +6.9 <i>i</i>	0.7 +0.7 <i>i</i>
$\pi^0\Sigma^0$	0.1 -1.6 <i>i</i>	1.7 -0.3 <i>i</i>	0.2 -0.2 <i>i</i>	1.8 +0.5 <i>i</i>	0.6 +0.2 <i>i</i>	0.1 -0.0 <i>i</i>
$\pi^+\Sigma^-$	-0.8 +0.5 <i>i</i>	0.0 +0.0 <i>i</i>	-0.1 -0.2 <i>i</i>	0.8 +0.1 <i>i</i>	0.2 -0.2 <i>i</i>	-0.2 +0.2 <i>i</i>
$\pi^-\Sigma^+$	0.5 -0.6 <i>i</i>	1.2 +0.4 <i>i</i>	0.1 +0.4 <i>i</i>	2.4 +2.4 <i>i</i>	-1.2 -0.6 <i>i</i>	-0.1 +0.2 <i>i</i>